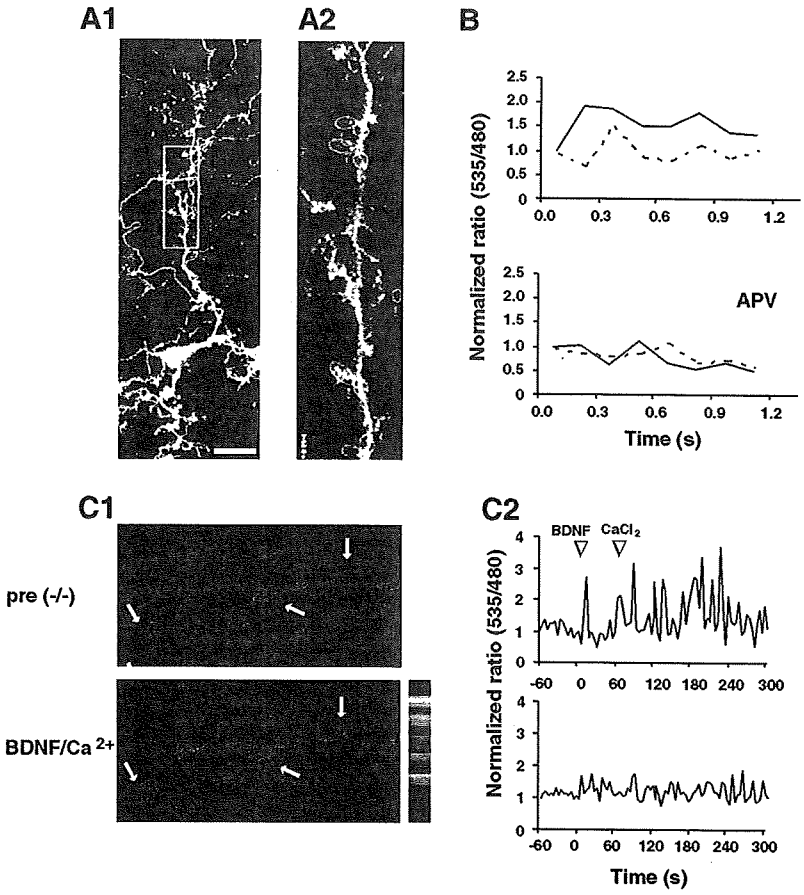

Fig. 1. Local calcium transients in spines and shafts of the longest dendrite in cortical pyramidal neurons after BDNF application or NMDAR stimulation. (A1) Confocal YFP image of a single cortical pyramidal cell expressing YC3.60 and YC3.60pm. The white box indicates the region shown at higher magnification in A2. Scale bar, 20 μm. (A2) Representative region of calcium imaging in spines and dendritic shafts (circled). (B) Representative traces of average calcium dynamics evoked by NMDAR stimulation by uncaging MNI-glutamate. Upper panel: the averaged tracing of time-lapse calcium imaging in five pairs of spine (bold line) and shaft (dashed line). Lower panel: the blockage of NMDAR-induced calcium transients by APV. Relative intracellular Ca^{2+} concentration is expressed as a ratio of YFP/CFP fluorescence, normalized to 1.0 at the start of the measurement before uncaging. Thus, just before uncaging at time 0, the ratio of YFP/CFP fluorescence equals 1. The time course in the presence of the caged glutamate but without photolysis was similar to that in the presence of APV (not shown). For measurements before time 0, at −50, −40, −30, −20, −10 s, the averaged ratio values were around 1 ± 0.16. (C1) Representative Ca^{2+} dynamics (averaged ratio of YFP/CFP fluorescence for each treatment condition) by pseudo-color representation: before BDNF application in nominally Ca^{2+}-free ECS (pre, −/−), and BDNF application with Ca^{2+} addition (BDNF/Ca^{2+}). Blue depicts low ratio, and red depicts high ratio as indicated in the colored bar. The arrows indicate some representative spines where Ca^{2+} increased. C2, Representative traces of calcium dynamics evoked by BDNF application obtained from a spine (bold line, upper panel) and the adjacent dendritic shaft (thin line, lower panel). Intracellular Ca^{2+} concentration was expressed as a ratio at each time point normalized with a value at −4 s set to 1.

similar in control and BDNF conditions: control, 282 ± 63 (n = 5, 22 spine-shaft pairs); BDNF, 298 ± 64 (n = 5, 22 pairs) for the integrated fluorescent intensity values that were normalized with the average intensity of cameleon in the same area.

Fixation with a conventional fixative such as 4% paraformaldehyde might permeabilize cell membranes and thus allow some antibody penetration. Thus, we could have overestimated the surface distribution of GluR1. In order to exclude this possibility, we first applied the GluR1 antibody to live cells at 4 °C, washed out the unbound antibody, then fixed the cells to process further for 2nd immunostaining. As a control experiment, we first fixed cells and treated the cells with the same antibody under the same conditions as for the live cell immunostaining (Fig. 3A). In both cases we observed a similar increment in the relative distribution of GluR1 between PSD and non-PSD regions after addition of BDNF. This result shows that our immunostaining conditions allow detection specifically of surface GluR1.

What is the origin of the additional synaptic GluR1? We considered lateral diffusion from the cell soma [25] or the local dendritic compartment as candidates [18,26,27]. To distinguish these possibilities, we transected dendrites from their soma as described in Experimental procedures. Isolated and intact spines/dendrites responded similarly (Fig. 3B, Cut control and Cut BDNF), suggesting that the effect of BDNF on AMPAR trafficking was local in the dendrite and not the consequence of action on the cell soma. In the process of silent synapse activation by BDNF, NMDAR function did not change, but that of AMPAR did [12]. We therefore examined

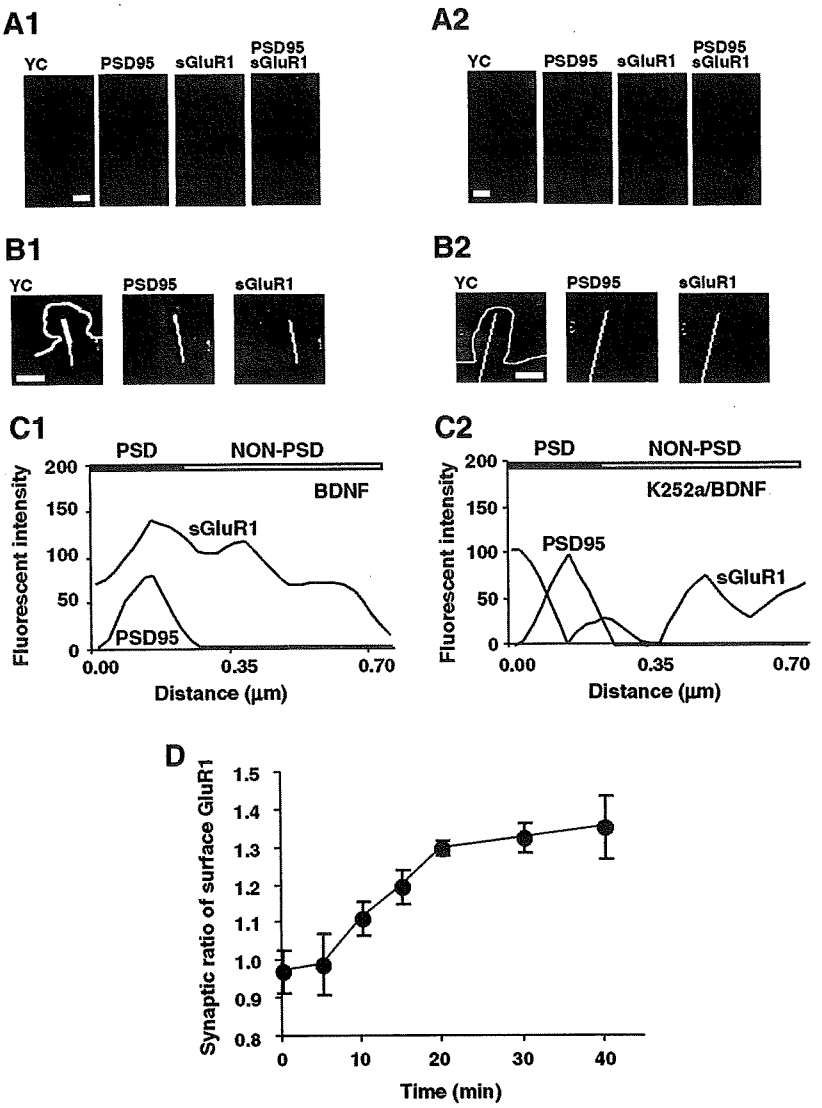

Fig. 2. Measurement of the surface expression of GluR1 at post-synaptic sites. A, Representative GluR1 and PSD95 staining in a dendrite treated with BDNF (A1), or Trk inhibitor K252a and BDNF (A2). YC: yellow cameleon; sGluR1: surface GluR1. Scale bar, 5 μm. (B and C) Representative line plot measurement of surface GluR1 across a spine and the adjacent dendritic shaft in a Ca^{2+} imaged-region. We drew a line that ran across the PSD-95 positive and negative region as shown by the bar (black and white) in C. (B1,C1) Representative traces of line plot measurement of BDNF-treated spine. (B2,C2) Representative traces of line plot measurement of K252a/BDNF-treated spine. Scale bar, 1 μm. D, Time course of changes in synaptic ratio of surface GluR1 by BDNF application. The details of the calculation for the synaptic ratio of surface GluR1 are described in Section 2. We repeated independent culture setups several times ("n" in the following) and measured the co-localization of GluR1 and PSD-95 with spine-shaft pairs from each culture setup (number of pairs shown in the parenthesis in the following). At each time point (min), n and number of pairs were $t = 0$, $n = 18$ (80 pairs); $t = 5$, $n = 7$, (43); t=10, $n = 7$ (43); $t = 15$, $n = 7$ (43); $t = 20$, $n = 7$, (46); $t = 30$, $n = 7$ (44); $t = 40$, $n = 24$ (111): The results are expressed as mean ± S.E.M.

the selectivity of the BDNF effect for AMPAR vs. NMDAR subunit NR1 translocation, and found no effect on the latter (Fig. 3C). In our present study, we focused on the primary dendrite and found the effect of BDNF was local. It has been reported that the post-Golgi secretory machinery (Golgi outposts) is preferentially directed to a single longest principal dendrite in hippocampal pyramidal neurons [28]. Therefore, it may be important to distinguish dendrite-type specific trafficking of AMPAR into synaptic densities.

It is well established that BDNF regulates the morphology of both axon terminals and dendrites [5,6]. Thus, the increment of surface GluR1 may be the consequence of an increase in pre- and post-synaptic contact. We tested this hypothesis by asking whether co-localization of pre- and post-synaptic markers, synaptophysin and PSD-95, increases upon BDNF addition. The extent of co-localization was the same with (70.3% ± 7.8 colocalized, $n = 4$) or without (72.4% ± 13.7, $n = 4$) BDNF (data not shown). This result is consistent with

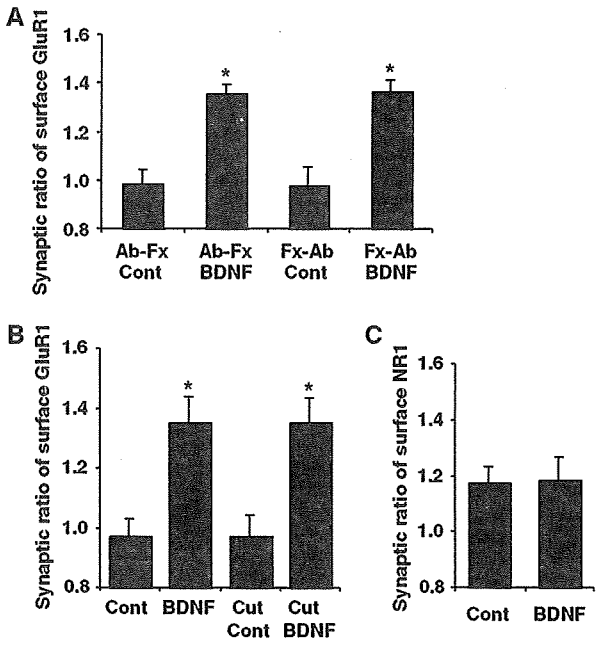

Fig. 3. Increment of the surface expression of GluR1 at post-synaptic density upon BDNF application. (A) Effect of the surface GluR1 immunostaining method on the synaptic ratio-value of surface GluR1 with live or fixed cells. For live-cell staining (Ab-Fx), neurons were washed with ECS after the end of stimulation, and the cell surface GluR1 was labeled with rabbit anti-GluR1 N-terminal antibody (JH1816) in 2% BSA/ECS for 30 min at 4 °C, followed by washing with ECS. The cells were fixed with 4% paraformaldehyde/4% sucrose, then further labeled with biotinylated anti-rabbit IgG and nanocrystal Qdot 605 streptavidin. For control condition of fixed cell-staining (Fx-Ab), the cells were washed with ECS and fixed with 4% paraformaldehyde/4% sucrose, followed by washing with ECS. The cell surface GluR1 was labeled with rabbit anti-GluR1 N-terminal antibody in 2% BSA/ECS for 30 min at 4 °C, followed by washing with ECS. The GluR1 was further labeled with biotinylated anti-rabbit IgG and nanocrystal Qdot 605 streptavidin. For both live- and fixed-cells procedures, after the staining of GluR1, cells were permeabilized with 0.25% Triton X-100 and post-synaptic density-95 (PSD-95) was stained by a monoclonal antibody (Upstate) and Cascade Blue conjugated anti-mouse IgG (Molecular Probes). The synaptic ratio of surface GluR1 was calculated as described in Section 2. The extent of increase in surface GluR1 expression at PSD by BDNF application was very similar between live cell staining and fixed cell staining. Live cell-staining/control (without stimulation): (Ab-Fx Cont), $n = 8$ (47 pairs); live cell-staining/BDNF: (Ab-Fx BDNF), $n = 8$ (47 pairs); fixed cell-staining/control: (Fx-Ab Cont), $n = 7$ (41 pairs); fixed cell-staining/BDNF:(Fx-Ab BDNF), $n = 7$ (40 pairs): The values n and the number of pairs defined as in Fig. 2 legend. Values are mean ± S.E.M., $^*P < 0.02$ relative to each control; t-test. (B) BDNF-induced translocation of local dendritic source of GluR1. Dendrites were separated from the soma as described in Section 2, and we examined the effect of BDNF application on translocation of surface GluR1. Control (without stimulation), $n = 18$ (80 pairs); BDNF, $n = 24$ (111 pairs); Cut (transected dendrite) control, $n = 6$ (33 pairs); Cut (transected dendrite) BDNF, $n = 6$ (34 pairs): mean ± S.E.M., $^*P < 0.01$ relative to control. (C) No change of synaptic ratio of surface NR1 by BDNF application. Control, $n = 8$ (45 pairs); BDNF, $n = 8$ (45 pairs): mean ± S.E.M. We used the time point of 40 min after BDNF addition to evaluate AMPAR translocation for most experiments except as otherwise indicated. This time is accepted as indicative of an LTP effect.

the idea that BDNF directly up-regulates GluR1 translocation at post-synaptic densities.

3.2. Spatially and temporally different Ca^{2+} sources contribute to the regulation of AMPAR trafficking by BDNF

Receptor tyrosine kinase TrkB mediates BDNF action to induce a subset of signaling pathways including Ras-ERK, phosphatidilinositol-3 kinase (PI3K), and phospholipase C (PLC) γ[29]. Among these, PLCγ activation is known to induce increases in intracellular Ca^{2+} and protein kinase C (PKC) activation. We therefore examined the PLCγ pathway to understand the mechanism of BDNF regulation of AMPAR trafficking at the post-synaptic membranes. We first confirmed that pharmacological inhibition of receptor tyrosine kinase TrkB by K252a (20 nM) blocked Ca^{2+} transients in dendritic spine-shaft pairs (Fig. 4A). Similarly, a selective PLCγ inhibitor, U73122 (1 μM) inhibited the BDNF effect (Fig. 4A), while an inactive counterpart, U73343 (1 μM), did not (not shown). A specific inhibitor of IP3R, Xestospongin C (Xest C), blocked all Ca^{2+} transients, both efflux from intracellular stores and influx through plasma membranes (Fig. 4A). TRPC3 channels are highly expressed in the developing brain, including in cortical pyramidal neurons, with a pattern of expression paralleling that of TrkB both temporally and spatially [30]. Indeed, the immunocytochemical staining revealed that TRPC3/6/7 subfamily channels were expressed at dendrites and spines of cortical pyramidal neurons with partial co-localization with surface GluR1 (Fig. 4C) irrespective of BDNF treatment. BDNF treatment increased the co-localization of TRPC and PSD-95 (Fig. 4D). We then tested the effect of SKF96365, an inhibitor of store-operated cation channels including TRPC. The Ca^{2+} transient evoked by BDNF in the presence of 2 mM $CaCl_2$ was significantly blocked by SKF96365 (30 μM). In contrast, little effect was observed on the first Ca^{2+} transient induced by BDNF in the nominally Ca^{2+}-free extracellular solution (Fig. 4A). At the same time, we measured the synaptic ratio of surface GluR1 in the presence of various inhibitors. The effect of each inhibitor on the synaptic ratio of surface GluR1 paralleled its effect on Ca^{2+} transients (Fig. 4B). Another antagonist of IP3R and SOC (store-operated channel), 2-APB (50 μM), showed the same effect as Xest C (Fig. 4B). Furthermore, GF109203X (50 nM), a specific inhibitor of a subset of protein kinase C isoforms, showed little effect on BDNF-induced GluR1 trafficking (Fig. 4B), whereas SKF96365 inhibited the increase of surface expression of GluR1 by BDNF (about 60%) (Fig. 4B). La^{3+} (100 μM), which inhibits many cation channels including TRPC, showed the same effect as SKF96365 (Fig. 4B). These results suggest that the Ca^{2+} transients caused by the release of Ca^{2+} from internal stores triggered a calcium signaling cascade including the TRPC channel acting downstream, and that AMPA receptor trafficking by BDNF into post-synaptic densities needs both types of Ca^{2+} transients. NMDAR stimulation also induced synaptic translocation of GluR1, probably through a calcium signaling pathway different from that evoked by BDNF (see Supplementary Fig. 1), since the effect of NMDAR and TrkB stimulation was additive.

3.3. Downstream signaling of Ca^{2+} transients evoked by BDNF

The number of synaptic AMPAR is determined by the balance between insertion and removal of receptors at post-synaptic membranes [31–33]. The trafficking mechanism of AMPAR has been intensively studied, but it is very complex process and the whole picture is still uncertain. The regulation

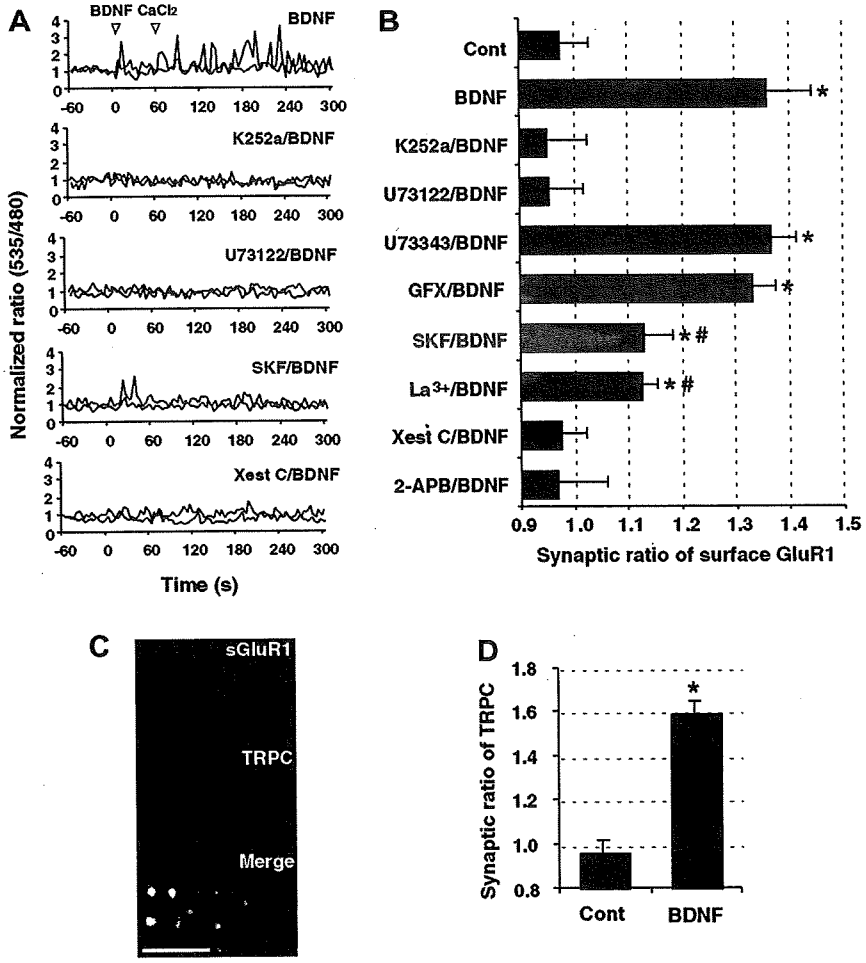

Fig. 4. Increment of post-synaptic expression of GluR1 by BDNF activation of diverse Ca^{2+} signaling cascades. (A, B) The role of TrkB/PLCγ and downstream Ca^{2+} signaling cascade on GluR1 expression at synapses. (A) Representative traces of Ca^{2+} dynamics in a spine (bold line) and the adjacent dendritic shaft (thin line). BDNF was applied at time 0 in nominally Ca^{2+}-free saline, followed by the addition of 2 mM $CaCl_2$ at 60 s. K252a, U73122 and a subset of channel inhibitor blocked the calcium dynamics. The control time course in the ECS medium was similar to K252a/BDNF. B. The effect of BDNF on synaptic ratio of surface GluR1 was attenuated by inhibition of the TrkB/PLCγ cascade or of a subset of Ca^{2+} channels. The TrkB inhibitor K252a, and the PLCγ inhibitor U73122, but not the PKC inhibitor GF109203X, blocked the effect of BDNF. The BDNF effect was partially blocked by La^{3+} and SKF96365, an inhibitor of store-operated cation channels including TRPC, whereas the IP3R inhibitors Xest C and 2-APB blocked almost completely. Control, $n = 18$ (80 pairs); BDNF, $n = 24$ (111); K252a + BDNF, $n = 9$ (48); U73122 + BDNF, $n = 9$ (48), U73343 + BDNF, $n = 7$ (36); GF109203X + BDNF, $n = 8$ (44); SKF96365 + BDNF, $n = 9$ (42); La^{3+} + BDNF, $n = 7$ (40); XestC+BDNF, $n = 8$ (36); 2-APB + BDNF, $n = 7$ (40): mean ± S.E.M., $^{*}P < 0.01$ relative to control, $^{\#}P < 0.01$ relative to BDNF for SKF96365 + BDNF or La^{3+} + BDNF; *t*-test. (C, D) Expression of endogenous TRPC3/6/7 channels in dendrites of cortical pyramidal neurons. (C) Coexpression of endogenous GluR1 at the surface of a dendrite (red: Qdot 605:upper panel) and endogenous TRPC3/6/7 channels (green: Qdot 655:middle panel). The merged image is shown (bottom panel) in the CFP (blue) expressing neuron with BDNF application. Scale bar, 5 μm. (D) BDNF treatment increased the localization of TRPC3/6/7 near the PSD by about 60% over the control, as assessed by measuring the overlap with PSD-95. Control, $n = 8$ (40 pairs); BDNF, $n = 8$ (40 pairs): mean ± S.E.M., $^{*}P < 0.01$ relative to control; *t*-test.

is different among the subunit types GluR1 and GluR2/3, and dependent on neuronal cell type as well. Ras family GTPases [34–38], Rab family GTPases [26,27], adenylyl cyclase I [39] and PI3 kinase [40] have been implicated in the regulation of AMPAR trafficking. The actin cytoskeleton [41], PDZ proteins [42–45], and a family of small transmembrane AMPA receptor regulatory proteins (TARPs) [46] have also been demonstrated to contribute to AMPAR turnover and translocation. Recently, it was reported that IP3R-mediated Ca^{2+} release can enhance AMPAR EPSC amplitudes through mechanisms that involve AMPAR-PDZ interactions and/or synaptotagmin-SNARE-mediated receptor trafficking [47]. In this paper, we focused on the signaling mechanisms downstream of TrkB/PLCγ activated by BDNF. Our data suggest that IP3-mediated internal store and TRPC-mediated influx may regulate different processes of AMPAR trafficking within the local spine compartment. Ca^{2+} regulates PICK1 sensor leading to internalization of GluR2 [43], activates NO production and thus up-regulates GluR2 together with GRIP1/Neep21 [44], or activates calmodulin in turn activating type I adenylyl cyclase (AC1) leading to GluR1 phosphorylation by PKA and up-regulation of GluR1 [39]. In our study, a PKC inhibitor was not effective, but a PKA may be involved downstream of the TRPC signaling pathway [48].

We used immunocytochemical analyses to measure the translocation of endogenous AMPAR in dendrites and synapses, as was done previously by others [26,27]. This method is advantageous to study the movement of endogenous protein. However, in the next step we need time lapse analysis in the three-dimensional space of dendrite/spine in order to reveal the dynamic process of AMPAR movements in synapses using conditional fluorescent dyes like tetracysteine targeting moieties [49]. A chronic up-regulation of BDNF mRNA and sequential increase of synaptic AMPARs in rat hippocampus have been seen after chronic antidepressant treatment [50]. Changes of BDNF/TrkB signaling and the related AMPAR trafficking may be involved in a variety of neurological and psychiatric disorders, and the understanding of the detailed mechanisms of BDNF regulation of AMPAR translocation at synapses may suggest new treatments for a subset of neuronal dysfunctions.

Acknowledgements: This study was supported by health sciences research grant of nano-1. We thank Drs. T. Nagai and A. Miyawaki for providing plasmids for yellow cameleon, Dr. R. Huganir for GluR1 N-terminal antibody, and Dr. M. Watanabe for PSD-95 polyclonal antibody.

Appendix A. Supplementary data

Supplementary data associated with this article can be found, in the online version, at doi:10.1016/j.febslet.2007.04.041.

References

[1] Klein, R. (1994) Role of neurotrophins in mouse neuronal development. FASEB J. 8, 738–744.
[2] Thoenen, H. (1995) Neurotrophins and neuronal plasticity. Science 270, 593–598.
[3] Katz, L.C. and Shatz, C.J. (1996) Synaptic activity and the construction of cortical circuits. Science 274, 1133–1138.
[4] Levi-Montalcini, R., Skaper, S.D., Dal Toso, R., Petrelli, L. and Leon, A. (1996) Nerve growth factor: from neurotrophin to neurokine. Trends Neurosci. 19, 514–520.
[5] Cline, H.T. (2001) Dendritic arbor development and synaptogenesis. Curr. Opin. Neurobiol. 11, 118–126.
[6] Poo, M.M. (2001) Neurotrophins as synaptic modulators. Nat. Rev. Neurosci. 2, 24–32.
[7] Kohara, K., Kitamura, A., Morishima, M. and Tsumoto, T. (2001) Activity-dependent transfer of brain-derived neurotrophic factor to postsynaptic neurons. Science 291, 2419–2423.
[8] Figurov, A., Pozzo-Miller, L.D., Olafsson, P., Wang, T. and Lu, B. (1996) Regulation of synaptic responses to high-frequency stimulation and LTP by neurotrophins in the hippocampus. Nature 381, 706–709.
[9] Kang, H., Welcher, A.A., Shelton, D. and Schuman, E.M. (1997) Neurotrophins and time: different roles for TrkB signaling in hippocampal long-term potentiation. Neuron 19, 653–664.
[10] Kovalchuk, Y., Hanse, E., Kafitz, K.W. and Konnerth, A. (2002) Postsynaptic induction of BDNF-mediated long-term potentiation. Science 295, 1729–1734.
[11] Minichiello, L. et al. (1999) Essential role for TrkB receptors in hippocampus-mediated learning. Neuron 24, 401–414.
[12] Itami, C., Kimura, F., Kohno, T., Matsuoka, M., Ichikawa, M., Tsumoto, T. and Nakamura, S. (2003) Brain-derived neurotrophic factor-dependent unmasking of "silent" synapses in the developing mouse barrel cortex. Proc. Natl. Acad. Sci. USA 100, 13069–13074.
[13] Narisawa-Saito, M., Iwakura, Y., Kawamura, M., Araki, K., Kozaki, S., Takei, N. and Nawa, H. (2002) Brain-derived neurotrophic factor regulates surface expression of alpha-amino-3-hydroxy-5-methyl-4-isoxazolepropionic acid receptors by enhancing the *N*-ethylmaleimide-sensitive factor/GluR2 interaction in developing neocortical neurons. J. Biol. Chem. 277, 40901–40910.
[14] Jourdi, H. et al. (2003) Brain-derived neurotrophic factor signal enhances and maintains the expression of AMPA receptor-associated PDZ proteins in developing cortical neurons. Dev. Biol. 263, 216–230.
[15] Hering, H. and Sheng, M. (2001) Dendritic spines: structure, dynamics and regulation. Nat. Rev. Neurosci. 2, 880–888.
[16] Noguchi, J., Matsuzaki, M., Ellis-Davies, G.C. and Kasai, H. (2005) Spine-neck geometry determines NMDA receptor-dependent Ca^{2+} signaling in dendrites. Neuron 46, 609–622.
[17] Bloodgood, B.L. and Sabatini, B.L. (2005) Neuronal activity regulates diffusion across the neck of dendritic spines. Science 310, 866–869.
[18] Shi, S.H., Hayashi, Y., Petralia, R.S., Zaman, S.H., Wenthold, R.J., Svoboda, K. and Malinow, R. (1999) Rapid spine delivery and redistribution of AMPA receptors after synaptic NMDA receptor activation. Science 284, 1811–1816.
[19] Hayashi, Y., Shi, S.H., Esteban, J.A., Piccini, A., Poncer, J.C. and Malinow, R. (2000) Driving AMPA receptors into synapses by LTP and CaMKII: requirement for GluR1 and PDZ domain interaction. Science 287, 2262–2267.
[20] Passafaro, M., Piech, V. and Sheng, M. (2001) Subunit-specific temporal and spatial patterns of AMPA receptor exocytosis in hippocampal neurons. Nat. Neurosci. 4, 917–926.
[21] Shi, S., Hayashi, Y., Esteban, J.A. and Malinow, R. (2001) Subunit-specific rules governing AMPA receptor trafficking to synapses in hippocampal pyramidal neurons. Cell 105, 331–343.
[22] Kakegawa, W., Tsuzuki, K., Yoshida, Y., Kameyama, K. and Ozawa, S. (2004) Input- and subunit-specific AMPA receptor trafficking underlying long-term potentiation at hippocampal CA3 synapses. Eur. J. Neurosci. 20, 101–110.
[23] Nagai, T., Yamada, S., Tominaga, T., Ichikawa, M. and Miyawaki, A. (2004) Expanded dynamic range of fluorescent indicators for Ca^{2+} by circularly permuted yellow fluorescent proteins. Proc. Natl. Acad. Sci. USA 101, 10554–10559.
[24] Matsuzaki, M., Honkura, N., Ellis-Davies, G.C. and Kasai, H. (2004) Structural basis of long-term potentiation in single dendritic spines. Nature 429, 761–766.
[25] Adesnik, H., Nicoll, R.A. and England, P.M. (2005) Photoinactivation of native AMPA receptors reveals their real-time trafficking. Neuron 48, 977–985.
[26] Park, M., Penick, E.C., Edwards, J.G., Kauer, J.A. and Ehlers, M.D. (2004) Recycling endosomes supply AMPA receptors for LTP. Science 305, 1972–1975.
[27] Gerges, N.Z., Backos, D.S. and Esteban, J.A. (2004) Local control of AMPA receptor trafficking at the postsynaptic terminal by a small GTPase of the Rab family. J. Biol. Chem. 279, 43870–43878.
[28] Horton, A.C., Racz, B., Monson, E.E., Lin, A.L., Weinberg, R.J. and Ehlers, M.D. (2005) Polarized secretory trafficking directs cargo for asymmetric dendrite growth and morphogenesis. Neuron 48, 757–771.
[29] Huang, E.J. and Reichardt, L.F. (2003) Trk receptors: roles in neuronal signal transduction. Annu. Rev. Biochem. 72, 609–642.
[30] Li, H.S., Xu, X.Z. and Montell, C. (1999) Activation of a TRPC3-dependent cation current through the neurotrophin BDNF. Neuron 24, 261–273.
[31] Malinow, R. and Malenka, R.C. (2002) AMPA receptor trafficking and synaptic plasticity. Annu. Rev. Neurosci. 25, 103–126.
[32] Ehlers, M.D. (2000) Reinsertion or degradation of AMPA receptors determined by activity-dependent endocytic sorting. Neuron 28, 511–525.
[33] Triller, A. and Choquet, D. (2005) Surface trafficking of receptors between synaptic and extrasynaptic membranes: and yet they do move! Trends Neurosci. 28, 133–139.
[34] Zhu, J.J., Qin, Y., Zhao, M., Van Aelst, L. and Malinow, R. (2002) Ras and Rap control AMPA receptor trafficking during synaptic plasticity. Cell 110, 443–455.
[35] Krapivinsky, G. et al. (2003) The NMDA receptor is coupled to the ERK pathway by a direct interaction between NR2B and RasGRF1. Neuron 40, 775–784.

[36] Krapivinsky, G., Medina, I., Krapivinsky, L., Gapon, S. and Clapham, D.E. (2004) SynGAP-MUPP1-CaMKII synaptic complexes regulate p38 MAP kinase activity and NMDA receptor-dependent synaptic AMPA receptor potentiation. Neuron 43, 563–574.
[37] Kim, M.J., Dunah, A.W., Wang, Y.T. and Sheng, M. (2005) Differential roles of NR2A- and NR2B-containing NMDA receptors in Ras-ERK signaling and AMPA receptor trafficking. Neuron 46, 745–760.
[38] Zhu, Y. et al. (2005) Rap2-JNK removes synaptic AMPA receptors during depotentiation. Neuron 46, 905–916.
[39] Lu, H.C., She, W.C., Plas, D.T., Neumann, P.E., Janz, R. and Crair, M.C. (2003) Adenylyl cyclase I regulates AMPA receptor trafficking during mouse cortical 'barrel' map development. Nat. Neurosci. 6, 939–947.
[40] Man, H.Y. et al. (2003) Activation of PI3-kinase is required for AMPA receptor insertion during LTP of mEPSCs in cultured hippocampal neurons. Neuron 38, 611–624.
[41] Zhou, Q., Xiao, M. and Nicoll, R.A. (2001) Contribution of cytoskeleton to the internalization of AMPA receptors. Proc. Natl. Acad. Sci. USA 98, 1261–1266.
[42] Cuadra, A.E., Kuo, S.H., Kawasaki, Y., Bredt, D.S. and Chetkovich, D.M. (2004) AMPA receptor synaptic targeting regulated by stargazin interactions with the Golgi-resident PDZ protein nPIST. J. Neurosci. 24, 7491–7502.
[43] Hanley, J.G. and Henley, J.M. (2005) PICK1 is a calcium-sensor for NMDA-induced AMPA receptor trafficking. EMBO J. 24, 3266–3278.
[44] Huang, Y. et al. (2005) S-nitrosylation of *N*-ethylmaleimide sensitive factor mediates surface expression of AMPA receptors. Neuron 46, 533–540.
[45] Steiner, P. et al. (2005) Interactions between NEEP21, GRIP1 and GluR2 regulate sorting and recycling of the glutamate receptor subunit GluR2. EMBO J. 24, 2873–2884.
[46] Nicoll, R.A., Tomita, S. and Bredt, D.S. (2006) Auxiliary subunits assist AMPA-type glutamate receptors. Science 311, 1253–1256.
[47] Maher, B.J., Mackinnon 2nd, R.L., Bai, J., Chapman, E.R. and Kelly, P.T. (2005) Activation of postsynaptic Ca^{2+} stores modulates glutamate receptor cycling in hippocampal neurons. J. Neurophysiol. 93, 178–188.
[48] Nakata, H. et.al. (2006) Brain-derived neurotrophic factor regulates AMPA receptor translocation to postsynaptic sites via adenylyl cyclase/protein kinase A and ERK signaling. In: Society for Neuroscience 36th Annual Meeting, # 423.7, Atlanta, USA.
[49] Ju, W. et al. (2004) Activity-dependent regulation of dendritic synthesis and trafficking of AMPA receptors. Nat. Neurosci. 7, 244–253.
[50] Martinez-Turrillas, R., Del Rio, J. and Frechilla, D. (2005) Sequential changes in BDNF mRNA expression and synaptic levels of AMPA receptor subunits in rat hippocampus after chronic antidepressant treatment. Neuropharmacology 49, 1178–1188.

Available online at www.sciencedirect.com
ScienceDirect
Neurochemistry International 50 (2007) 119–129
NEUROCHEMISTRY International
www.elsevier.com/locate/neuint

Dopaminergic neuronal loss in transgenic mice expressing the Parkinson's disease-associated UCH-L1 I93M mutant

Rieko Setsuie [a,b,1], Yu-Lai Wang [a,1], Hideki Mochizuki [c,d], Hitoshi Osaka [a,e], Hideki Hayakawa [c], Nobutsune Ichihara [f], Hang Li [a], Akiko Furuta [a], Yae Sano [a,b], Ying-Jie Sun [a], Jungkee Kwon [a,g], Tomohiro Kabuta [a], Kenji Yoshimi [d], Shunsuke Aoki [a], Yoshikuni Mizuno [c,d], Mami Noda [b], Keiji Wada [a,*]

[a] *Department of Degenerative Neurological Diseases, National Institute of Neuroscience, National Center of Neurology and Psychiatory, Kodaira, Tokyo 187-8502, Japan*
[b] *Laboratory of Pathophysiology, Graduate School of Pharmaceutical Sciences, Kyushu University, Higashi-ku, Fukuoka 812-8582, Japan*
[c] *Department of Neurology, Juntendo University School of Medicine, Bunkyo-ku, Tokyo 113-8421, Japan*
[d] *Research Institute for Diseases of Old Age, Juntendo University School of Medicine, Bunkyo-ku, Tokyo 113-8421, Japan*
[e] *Division of Neurology, Clinical Research Institute, Kanagawa Children's Medical Center, Yokohama 232-8555, Japan*
[f] *Department of Anatomy, School of Veterinary Medicine, Azabu University, Sagamihara 229-8501, Japan*
[g] *College of Veterinary Medicine, Chonbuk National University, 644-14 Duckjin-Ku, Jeonju 561-756, Republic of Korea*

Received 14 March 2006; received in revised form 19 June 2006; accepted 11 July 2006
Available online 11 September 2006

Abstract

The I93M mutation in ubiquitin carboxyl-terminal hydrolase L1 (UCH-L1) was reported in one German family with autosomal dominant Parkinson's disease (PD). The causative role of the mutation has, however, been questioned. We generated transgenic (Tg) mice carrying human *UCHL1* under control of the *PDGF-B* promoter; two independent lines were generated with the I93M mutation (a high- and low-expressing line) and one line with wild-type human UCH-L1. We found a significant reduction in the dopaminergic neurons in the substantia nigra and the dopamine content in the striatum in the high-expressing I93M Tg mice as compared with non-Tg mice at 20 weeks of age. Although these changes were absent in the low-expressing I93M Tg mice, 1-methyl-4-phenyl-1,2,3,6-tetrahydropyridine (MPTP) treatment profoundly reduced dopaminergic neurons in this line as compared with wild-type Tg or non-Tg mice. Abnormal neuropathologies were also observed, such as silver staining-positive argyrophilic grains in the perikarya of degenerating dopaminergic neurons, in I93M Tg mice. The midbrains of I93M Tg mice contained increased amounts of insoluble UCH-L1 as compared with those of non-Tg mice, perhaps resulting in a toxic gain of function. Collectively, our data represent *in vivo* evidence that expression of $UCHL1^{I93M}$ leads to the degeneration of dopaminergic neurons.

Keywords: Ubiquitin carboxy-terminal hydrolase L1; Animal model; Parkinson's disease; Dopaminergic neuron

1. Introduction

Parkinson's disease (PD) is the second most common human neurodegenerative disorder after Alzheimer's disease (AD) (Dauer and Przedborski, 2003; Vila and Przedborski, 2004). PD patients exhibit motor dysfunction, including slowed movement (bradykinesia), resting tremor, rigidity, and postural instability (Dauer and Przedborski, 2003). The pathological basis of PD is the progressive loss of dopaminergic neurons in the substantia nigra pars compacta, giving rise to a decrease in dopamine content in the striatum (Dauer and Przedborski, 2003). Although most cases of PD are sporadic, studies of familial PD have provided accumulating evidence for the molecular mechanisms of PD. Thus far, at least six proteins have been identified to cause familial PD: α-synuclein (Chartier-Harlin et al., 2004; Farrer et al., 2004; Ibanez et al., 2004; Kruger et al., 1998; Polymeropoulos et al., 1997; Singleton et al., 2003), UCH-L1 (Leroy et al., 1998), parkin (Kitada et al., 1998), DJ-1 (Bonifati et al., 2003), phosphatase

* Corresponding author. Tel.: +81 42 346 1715; fax: +81 42 346 1745.
E-mail address: wada@ncnp.go.jp (K. Wada).
[1] These authors contributed equally to this work.

0197-0186/$ – see front matter © 2006 Elsevier Ltd. All rights reserved.
doi:10.1016/j.neuint.2006.07.015

and tensin homolog induced kinase-1 (PINK1) (Valente et al., 2004), and leucine-rich repeat kinase-2 (LRRK2) (Paisan-Ruiz et al., 2004; Zimprich et al., 2004). α-Synuclein, UCH-L1 and LRRK2 are linked to the autosomal dominant form of PD, whereas parkin, DJ-1 and PINK1 are linked to the recessive form.

In 1998, UCH-L1 carrying an Ile to Met mutation at amino acid position 93 (I93M) was identified in one German family affected by autosomal dominant familial PD. UCH-L1, also known as PGP9.5, is an abundant protein in neuronal cells, comprising up to about 1–2% of total protein in the brain. Its function as de-ubiquitylating enzyme (Larsen et al., 1998; Wilkinson et al., 1989), ubiquitylating enzyme (Liu et al., 2002), de-neddylating enzyme (Hemelaar et al., 2004), and mono-ubiquitin stabilizer (Osaka et al., 2003) has been reported. *In vitro* analysis using recombinant human UCH-L1 indicated that I93M mutation results in the reduction of hydrolase activity of about 50% (Nishikawa et al., 2003). *Uchl1* gene deletion in mice, however, was reported to causes gracile axonal dystrophy (*gad*), a recessive neurodegenerative disease with distinct phenotype and pathological features from PD (Saigoh et al., 1999). Moreover, extensive analysis failed to find other PD patients with mutations in the *UCHL1* gene (Lincoln et al., 1999; Maraganore et al., 1999) and there was an incomplete penetrance in reported German family (Leroy et al., 1998). Thus, the correlation of I93M mutation and pathogenesis of PD was questioned.

To elucidate the pathological role of UCH-L1^{I93M} expression in the pathogenesis of PD, *in vivo*, we generated transgenic mice expressing human UCH-L1^{I93M}.

2. Experimental procedures

2.1. Generation of hUCHL1^{WT} and hUCHL1^{I93M} transgenic mice

We generated transgenes by cloning either the wild-type or I93M mutant human UCH-L1 cDNAs under the control of the human platelet-derived growth factor B chain (*PDGF-B*) promoter (Fig. 1A) (Sasahara et al., 1991). Sequences encoding *UCHL1* were amplified from a human brain cDNA library (Stratagene, La Jolla, CA) by PCR and subcloned into the *Xho*I and *Not*I sites of pCI-neo (Promega, Madison, WI). The I93M substitution was obtained using QuikChange (Stratagene). The 5′ flanking region of the human *PDGF-B* chain gene was isolated from the human genomic DNA and inserted into the *Bgl*II and *Xho*I site of pCI-neo which results in the replacement of promoter from CMV to *PDGF-B*. The plasmid was linearized by digestion with *Hin*dIII and *Aat*II. A 2 μg/ml solution of the linearized plasmid of each transgene was then microinjected into the pronuclei of newly fertilized C57BL/6J mouse eggs. Offspring were screened for the presence of the transgene by PCR of tail DNA using specific primers (forward: PD-UCH-2, 5′-GCACTCTCCCTTCTCCTTTATA-3′; reverse: PD-UCH-5, 5′-CCTGTATGGCCTCATTCTTTTC-3′). Expression of hUCH-L1^{I93M} in a low-expressing mouse line only occurred in male mice. Thus, all experiments were done using male heterozygous transgenic mice. Animal care and handling were in accordance with institutional regulations for animal care and were approved by the Animal Investigation Committee of the National Institute of Neuroscience, National Center of Neurology and Psychiatry, Tokyo, Japan which conforms the National Institute of Health guide for the care and use of Laboratory animals.

2.2. Quantitative RT-PCR analysis

Primers specific for mouse *Uchl1* (forward: mL1-7, 5′-CCTTGGTTTGCAG-CTTTAGCA-3′; reverse: mL1-8, 5′-GGGCTGTAGAACGCAAGAAGA-3′) and human *UCHL1* (forward: L1Tg-F2, 5′-TGGCAACTTCTCCTCCTGCA-3′; reverse: L1Tg-R2, 5′-ACAGCACTTTGTTCAGCATC-3′) were designed, and SYBR Green-based real-time quantitative RT-PCR was performed using the ABI PRISM 7700 (Applied Biosystems, Foster City, CA) using total RNA from mouse brain (n = 3 for each line) (Aoki et al., 2002). GAPDH was used as an internal control.

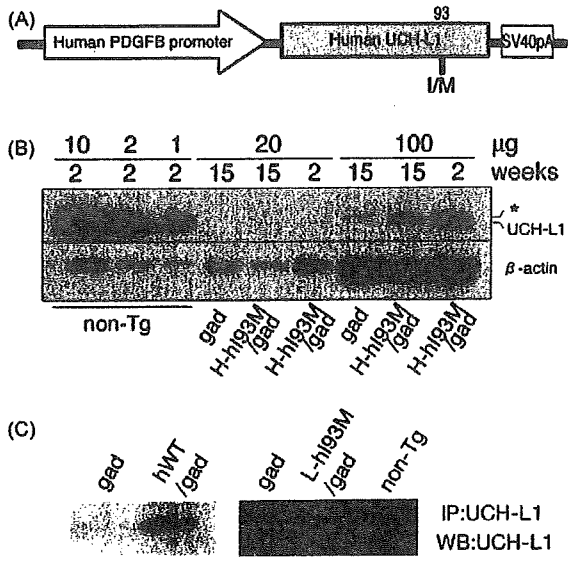

Fig. 1. Generation of transgenic mice expressing hUCH-L1^{WT}and hUCH-L1^{I93M}. (A) UCH-L1^{I93M} was constructed under control of the *PDGF-B* promoter, as depicted. (B) Immunoblotting analysis of endogenous mouse UCH-L1 and transgenic human UCH-L1 expression in mouse midbrain. To detect exogenous human UCH-L1 levels specifically, we generated transgenic mice in the *gad* background (H-hI93M/*gad*), which corresponds to the null mutant of *Uchl1*. Notice that the faint band corresponding to UCH-L1 is detected at 2 weeks of age when 20 μg protein/lane was loaded for the detergent-soluble fraction of midbrain origin in H-hI93M/*gad* mice. When the applied protein was increased to 100 μg/lane, UCH-L1 was easily detected at 2 weeks in H-hI93M/*gad* mice, and UCH-L1 levels markedly decreased by age 15 weeks. Faint bands indicated by the asterisk may correspond to UCH-L3, which cross-reacted with the UCH-L1 antibody when a large amount of protein was loaded per lane. (C) Immunoprecipitation analysis of exogenous human UCH-L1 in hWT/gad (left) and L-hI93M/gad (right) brains. Brain lysates from hWT/gad (left) or L-hI93M/gad (right) were both immunoprecipitated and detected using anti-UCH-L1 antibody. The band corresponding to the UCH-L1 can be found in both hWT/gad and L-hI93M/gad lysates but not in gad lysates indicating the exogenous human UCH-L1 expression.

2.3. Fractionation and immunoblotting and immunoprecipitation

For the immunoblotting of total UCH-L1, the soluble fraction in RIPA (20 mM Tris–HCl, pH 7.5; 0.1% SDS; 1.0% (w/v) Triton X-100; 1.0% sodium deoxycholate) with Complete EDTA-Free Protease Inhibitors (Roche, Basel, Switzerland) was extracted from H-hI93M/*gad* ([high-expressing] *UCH-L1*$^{I93M/-}$, *Uchl1*$^{gad/gad}$), *gad* and non-Tg mouse midbrains. The extracted samples were loaded as indicated in Fig. 1.

For subfractionation, the cortex and hippocampus were removed from the midbrains of a H-hI93M mouse or a non-Tg littermate and bottom half under the aqueduct were used as the substantia nigra fraction. The fractionation method was modified from that of Kahle et al. (2001). Each sample was homogenized with 9 volumes of 5% SDS/TBS lysis buffer (50 mM Tris–HCl (pH 7.5), 150 mM NaCl, 5% SDS) with Complete EDTA-Free Protease Inhibitors using a 23G syringe. After three times of 10 s sonication, samples were ultra-centrifuged in 130,000 × g for 1 h, and the supernatant were pooled as 5% SDS fraction. The pellets were washed with 5% SDS/TBS solution once and further homogenized in 8 M urea/5% SDS/TBS lysis buffer

(8 M urea, 5% SDS, 50 mM Tris–HCl (pH 7.5), 150 mM NaCl) with 23G syringe. The resulting supernatant was used as 8 M urea/5% SDS fraction. The protein concentration was assessed by a DC-protein assay kit (Bio-Rad). 1.25 μg of 5% SDS fraction and 0.5 μg of 8 M urea/5% SDS fraction were subjected to SDS-PAGE using 15% gels (Perfect NT Gel; DRC, Tokyo, Japan). Anti-UCH-L1 (1:5000, RA95101; Ultraclone, Isle of Wight, UK) and anti-β-actin (1:5000, clone AC15; Sigma, St. Louis, MO) were used to detect each protein. Signals were detected using a chemiluminescent SuperSignal West Dura Extended Duration Substrate kit or West Femto Maximum Sensitivity Substrate kit (Pierce, Rochford, IL) and analyzed with a ChemiImager (Alpha Innotech, San Leandro, CA). For the internal control of 8 M urea/5% SDS fraction, 1 μg protein were dot blotted to PVDF membrane and stained with Ponceau S staining (Rane et al., 2004). Statistical analyses were conducted using the two-tailed Student's *t*-test with total of four samples for each group.

For the immunoprecipitation, half of the brain (for hWT/gad) or midbrain region (for L-hI93M/gad) were homogenized in 2 ml ice-cold modified RIPA buffer (50 mM Tris–HCl, pH 7.4; 1% (w/v) Nonidet P40; 0.25% sodium deoxycholate; 150 mM NaCl; 1 mM EDTA) with Complete EDTA-Free Protease Inhibitors and centrifuged at 16,000 × *g* at 4 °C for 20 min. The protein concentration of the resulting supernatants was determined with the Protein Assay Kit (Bio-Rad, Hercules, CA). Immunoprecipitation was performed with a Seize X Mammalian Immunoprecipitation kit (Pierce, Rockford, IL) with some modifications. Briefly, 300 μg of protein was added to a 50 μl slurry of immobilized protein G cross-linked with rabbit polyclonal anti-human UCH-L1 (AB1716; Chemicon, Temecula, CA) or normal rabbit IgG and rotated at 4 °C overnight. The samples were then washed three times with 500 μl of 0.1B buffer (20 mM Tris–HCl, pH 8.0; 0.1 M KCl; 5 mM $MgCl_2$; 10% (w/v) glycerol; 0.1% (w/v) Tween 20; 10 mM β-mercaptoethanol). Elution of samples was performed by adding 20 μl of 5× SDS-PAGE sample buffer, and samples were boiled at 100 °C for 5 min.

2.4. Immunohistochemistry, immunofluorescence and electron microscopy

Brain and peripheral (sciatic) nerve sections from 2-, 7- and 20-week-old mice were analyzed ($n = 3$ for each line) by immunocytochemistry as previously described (Wang et al., 2004; Watanabe et al., 1977) using antibodies to UCH-L1 (1:4000; RA95101, Ultraclone), TH (1:1000; Chemicon) and ubiquitin (1:1000; Sigma–Aldrich, St. Louis, MO). Antibody binding was detected with 3,3′-diaminobenzidine tetrachloride (DAB) or 3-amino-9-ethylcarbazole (AEC) as a peroxidase substrate or Alexa-488- or Alexa-568-conjugated secondary antibodies (Invitrogen, Carlsbad, CA). Sections were then counterstained with hematoxylin. Ultrastructural electron microscopic studies of the substantia nigra were performed as described (Watanabe et al., 1977) using midbrain sections.

2.5. MPTP treatment

For MPTP treatment, the mice received four injections of 30 mg/kg MPTP–HCl intraperitoneally (Research Biochemicals, Natick, MA) in saline at 24-h intervals (Mochizuki et al., 2001).

2.6. Tyrosine hydroxylase-positive cell counting and biochemical analysis

Samples for both histochemistry and biochemical analysis were obtained from the same mouse. Each animal was deeply anesthetized with pentobarbital and perfused transcardially with 10 ml of ice-cold phosphate-buffered saline, and the brain was removed and divided into forebrain and midbrain–hindbrain regions.

For the tyrosine hydroxylase (TH)-positive cell counting, midbrain–hindbrain was fixed with chilled 4% formaldehyde solution (pH 7.4). The procedure of TH-positive cell counting was described previously (Furuya et al., 2004) with minor modifications. Briefly, the substantia nigra was cut into serial sections (30 μm), and every third section was subjected to immunostaining for TH using a polyclonal antibody to TH (a kind gift from I. Nagatsu, Fujita Health University, Aichi, Japan). The Vectorstain Elite ABC kit (Vector Labs, Burlingame, CA) was used for subsequent antibody detection with DAB as a peroxidase substrate. The number of viable TH-positive neurons was assessed by manual counting by a blind observer using coded slides (Furuya et al., 2004). The number of total neuronal cells outside the substantia nigra was counted after Bodian staining in the cerebral cortex (1 mm^2, seven regions per section), cerebellum (total of all lobules) and hippocampus (total number in CA1, CA2, CA3 and dentate gyrus). Statistical analysis were done by one-way ANOVA followed by post hoc test (Fisher's PLSD).

For the biochemical analysis, the striatum was quickly dissected from the forebrain, and the striatal tissue samples were weighed (~30 mg) and homogenized in 10 volumes (w/v) of ice-cold 0.05 M sodium acetate (pH 6.0). Homogenates were centrifuged (18,000 × *g*, 10 min at 4 °C), and the supernatant was frozen immediately on dry ice and stored frozen at −80 °C until use.

For the striatal dopamine measurement, supernatant (50 μl) from the striatal lysate was mixed with an equal volume of 0.2 M perchloric acid containing 0.2 mM EDTA and centrifuged (18,000 × *g*, 10 min at 4 °C), and the supernatant was applied to an HPLC system. Chromatographic separation was achieved using a C18 reversed-phase column (150 mm × 4.6 mm i.d., Model S-100; TOSOH, Tokyo, Japan). The mobile phase (50 mM citrate, 50 mM NaH_2PO_4, 0.1 mM EDTA, 4.36 mM 1-heptanesulfonate, 2.35% acetonitrile, 5.72% MeOH, pH 2.5) was pumped through the chromatographic system at a rate of 1.0 ml/min. A Coulochem electrode array system (ESA Inc., MA) with eight coulometric electrodes was used to quantify the eluted catecholamines and their metabolites. Statistical analysis was done by one-way ANOVA followed by post hoc test (Fisher's PLSD).

TH activity was assayed following the method of Hooper (1997) with minor modifications (Hooper et al., 1997; Naoi et al., 1988). The incubation mixture contained 50 μl of diluted sample and included the following components in a total volume of 200 μl: 0.2 M sodium acetate (pH 6.0), 0.2 M glycerol, 20,000 U/ml catalase, 1.0 mM 6-MPH4, 4.0 U/ml dihydropteridine reductase, 1 mM NADPH and 200 μM L-tyrosine. Incubations were carried out at 37 °C for 10 min in a shaking water bath. Reactions were terminated by adding 600 μl of ice-cold 0.33 M perchloric acid, 17 mM EDTA including 50 pmol of α-methyl DOPA as the internal standard. The L-DOPA produced was extracted onto alumina, and the catechols were eluted with 0.16 M acetic acid followed by 0.02 M phosphoric acid. A sample incubated on ice instead of 37 °C was used as a blank. The amount of L-DOPA was quantified with the HPLC system, as mentioned above. Statistical analysis was done by one-way ANOVA.

2.7. Silver staining

Sixty-micrometer brain sections from 12-week-old mice ($n = 3$ for each group) were stained using FD NeuroSilver kit (FD Neuro-Technologies, Catonsville, MD) according to the manufacturer's protocol to detect argyrophilic grain-positive degenerating neurons.

2.8. Behavioral tests

H-hI93M mice and non-Tg littermates were used for all behavioral analyses. For the accelerated rota-rod test, 20–25-week-old mice were placed on the rod (Ohara, Japan) at a speed of 5 rpm, and the speed was accelerated to 50 rpm in 5 min. The length of time that each mouse was able to remain on the rod before falling was recorded. For the locomotor activity test, 11–13-week-old or 20–23-week-old mice were placed separately in a home cage 4 days before the beginning of analysis for habituation. Two to four mice were monitored at once for locomotor activity on the home cage monitor (Ohara, Japan) for 63 h beginning from 5:30 p.m. All mice were housed with a 12 h light/dark cycle, with the light cycle beginning at 8 a.m. The last 12 h of active night were used for the analysis. Mice were weighed after the analysis; there were no differences between the weights H-hI93M and non-Tg mice (data not shown). Statistical analyses were conducted using the two-tailed Student's *t*-test.

3. Results

3.1. Generation of transgenic mice expressing human *UCHL1*^{I93M} in neurons of the substantia nigra

The human *PDGF-B* promoter was used to drive expression of the human *UCHL1* in Tg mice (Fig. 1A) (Sasahara et al., 1991). Germline transmission of *hUCHL1*^{I93M} was obtained in two independent Tg mouse lines (denoted L-hI93M and H-hI93M, where L and H denote low and high expression, respectively). Germline transmission of *hUCHL1*^{WT} was obtained in one Tg mouse line (denoted hWT). The levels of transgenic mRNA and endogenous *Uchl1* mRNA were assessed by quantitative RT-PCR using primers designed to amplify specifically the *UCHL1* transgene and mouse *Uchl1*, respectively. The estimated relative expression of *UCHL1* among the transgenic lines was H-hI93M > hWT > L-hI93M. The ratio of endogenous mouse *Uchl1* transcripts to transgenic human *UCHL1* transcripts was 111 in H-hI93M, 739 in hWT and 6015 in L-hI93M ($n = 3$ for each line).

At the amino acid level, human and mouse UCH-L1 differ at only 11 discrete positions, and endogenous UCH-L1 is one of the most abundant protein in the brain. Therefore, we were not able to make distinction between the exogenous human UCH-L1 and endogenous mouse UCH-L1 in the brains of Tg mice (data not shown) using immunoblotting analysis with several antibodies against human UCH-L1 from different companies (Chemicon; UltraClone; Medac; Biogenesis). To ascertain the expression of transgene product, we used *gad* mice, which lack endogenous UCH-L1 (Saigoh et al., 1999). We mated mice

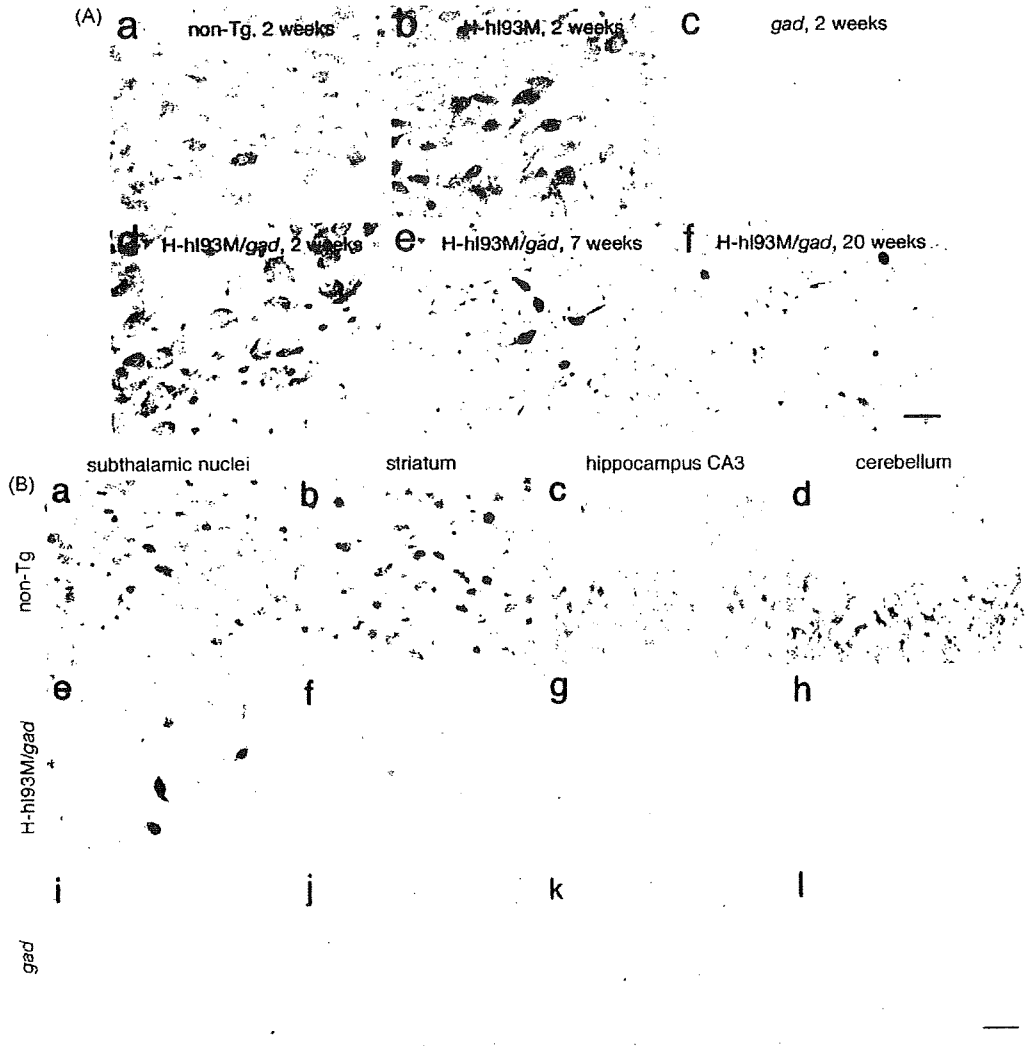

Fig. 2. Immunohistochemistry of UCH-L1 in coronal sections of the substantia nigra (A) and regions outside the substantia nigra (B) in H-hI93M, H-hI93M/*gad* and non-Tg mice. (A) Non-Tg mice (a), H-hI93M mice on a C57BL/6J background (b) and *gad* mice (c) at 2 weeks of age and H-hI93M/*gad* mice at 2 weeks (d), 7 weeks (e) and 20 weeks (f) of age. Neurons expressing UCH-L1 in the substantia nigra decreased in number and area, and densely stained neurons were observed in the aged substantia nigra. Scale bar: 30 μm. (B) UCH-L1 immunohistochemistry of coronal sections at the level of the subthalamic nuclei (a, e, i), striatum (b, f, j), hippocampus CA3 (c, g, k) and cerebellum (d, h, l). Upper row (a–d), non-Tg mice; middle row (e–h), H-hI93M/*gad* mice; lower row (i–l), *gad* mice. All mice were examined at 2 weeks of age. Scale bar: 30 μm.

from each transgenic line with mice homozygous for the *Uchl1*$^{gad/gad}$ allele (*gad* mice). Detergent-soluble (1% Triton X-100) fractions of mouse midbrain from H-hI93M/*gad* (*UCHL1*$^{I93M/-}$, *Uchl1*$^{gad/gad}$) at 2 and 15 weeks of age were subjected to SDS-PAGE and immunoblotted with anti-UCH-L1. We detected human UCH-L1 expression in H-hI93M/*gad* brains (Fig. 1B). Compared with endogenous mouse UCH-L1, which constitutes 1–2% of neuronal proteins, human UCH-L1 expression was substantially lower in H-hI93M/*gad* brains (~1% of endogenous UCH-L1 at 2 weeks of age; Fig. 1B). Interestingly, the level of transgenic human UCH-L1 was lower at 15 weeks than at 2 weeks of age (Fig. 1B). Although we could not detect human UCH-L1 in L-hI93M/*gad* and hWT/*gad* by standard immunoblotting methods, we were successful in detecting it by immunoprecipitation (Fig. 1C). These data suggest the expression of the human UCH-L1 in L-hI93M and hWT mice, which were much lower than in H-hI93M mice.

UCH-L1 is a cytosolic protein predominantly expressed in neuronal cells including dopaminergic neurons at substantia nigra with diffuse localization (data not shown). Thus, we next examined the immunohistochemical localization of the transgene products. In agreement with the data obtained by Western blotting analysis, UCH-L1-immunoreactive cells were not observed in any brain region, including the substantia nigra, of the L-hI93M/*gad* and hWT/*gad* mice (data not shown). In H-hI93M/*gad* mice, however, human UCH-L1^{I93M} was detected in the substantia nigra, the region that contains the central pathological lesions in PD, with relatively high intensities (Fig. 2A). Subthalamic nuclei, striatum, hippocampus CA3 and cerebellum also contained UCH-L1 immunoreactive cells in H-hI93M/*gad* mice (Fig. 2B). As with the previous report that CAT expression under control of the *PDGF-B* promoter in transgenic mice localizes to neuronal cell bodies (Sasahara et al., 1991), most UCH-L1-immunoreactive cells in H-hI93M/*gad* mice had a neuronal morphology (Fig. 2). Western blotting analysis of midbrain lysates showed a reduction of transgenic UCH-L1^{I93M} at 15 weeks of age as compared with that at 2 weeks in H-hI93M/*gad* mice (Fig. 1B). Thus, we also performed immunohistochemical analysis of UCH-L1 on substantia nigra from 2-, 7- and 20-week-old H-hI93M/*gad* mice. We found many UCH-L1-positive neurons at 2 weeks. The number of positive cells had decreased by 7 weeks, however, at which time small-sized and densely stained neurons were observed, and UCH-L1-positive cells were barely

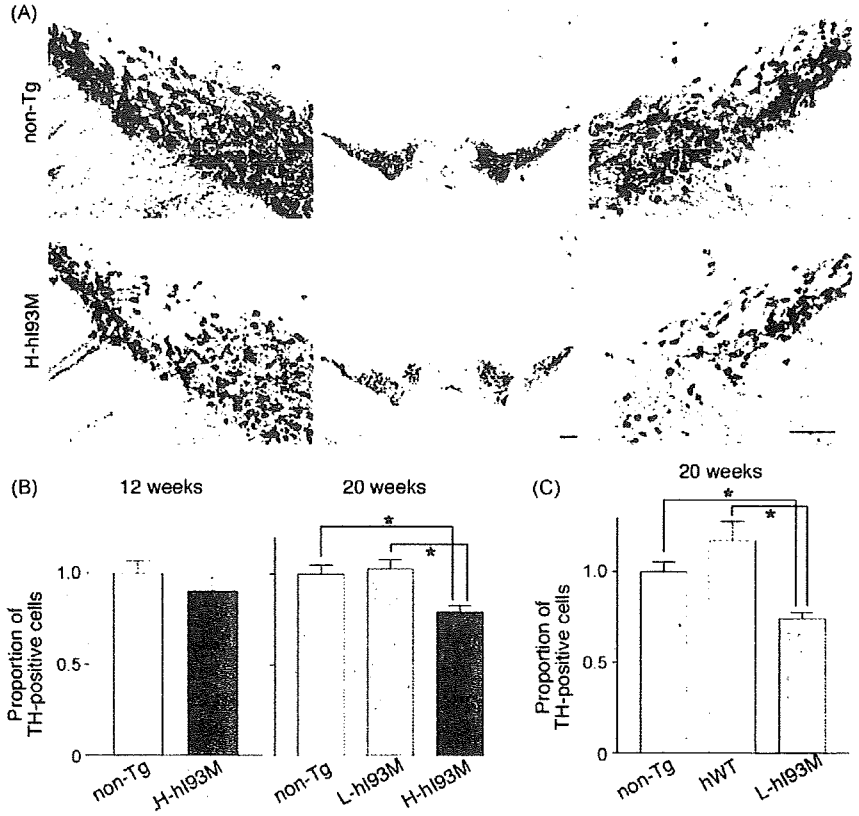

Fig. 3. TH-positive neurons of hI93M Tg mice were reduced as the animals aged. (A) Immunohistochemical staining of the substantia nigra with anti-TH in non-Tg (upper panels) and H-hI93M (lower panels) mice at 20 weeks of age. Scale bar: 1 mm. Left and right panels in the figure correspond to the left and right part of the middle panel, respectively. (B) Proportion of neurons stained with anti-TH in the substantia nigra from non-Tg and hI93M mice at 12 weeks (left panel) and 20 weeks (right panel) of age. Cell numbers were normalized to those for the non-Tg mice. Values are the mean ± S.E.M.; $n = 10$ Significance was examined by a one-way ANOVA. $^{*}p < 0.01$. (C) The number of TH-positive cells in the substantia nigra from 20-week-old non-Tg ($n = 5$), hWT ($n = 3$) and L-hI93M mice ($n = 5$) after treatment with MPTP. The cell numbers were normalized to those for non-Tg mice. Values are the mean ± S.E.M. Significance was examined by a one-way ANOVA. $^{*}p < 0.001$.

detectable at 20 weeks of age (Fig. 2A). Together, our results indicate that hUCH-L1^{I93M} is expressed in the neurons of the substantia nigra in H-hI93M mice, but the number of positive cells declines before 20 weeks of age. With the failure to detect hUCH-L1 protein in hWT/*gad* mice and L-hI93M/*gad* mice both in the Western blotting and the immunohistochemistry, we performed most of the analysis using H-hI93M mice with non-Tg mice as a control.

3.2. Loss of dopaminergic neurons in the substantia nigra of 20-week-old H-hI93M mice

We next determined whether the number of midbrain dopaminergic neurons was reduced in the substantia nigra of transgenic mice using TH immunohistochemistry. The number of TH-positive dopaminergic neurons in the substantia nigra at the same neuroanatomical level was compared and quantified for each transgenic mouse line. Surprisingly, we detected an ~30% reduction in TH-positive neurons in 20-week-old H-hI93M mice as compared with those in non-Tg control mice (Fig. 3A and B). This reduction was not seen in 12-week-old H-hI93M mice or 20-week-old L-hI93M mice. Together with the decrease in the level of UCH-L1^{I93M} (Fig. 1B) and the reduction in UCH-L1-positive neurons in the substantia nigra of H-hI93M/*gad* mice, our data indicate that UCH-L1^{I93M} expression in the dopaminergic neurons is sufficient to induce the degeneration of these neurons.

MPTP is a toxin used to induce an acute Parkinsonian syndrome that is indistinguishable from sporadic PD (Dauer and Przedborski, 2003). MPTP metabolite 1-methyl-4-pyridinium (MPP^+), an inhibitor of complex I of the mitochondrial respiration chain, is taken up by the terminals of dopaminergic neurons via the dopamine transporter (DAT), thereby causing the selective death of nigral neurons (Dauer and Przedborski, 2003). Although neuronal loss was not observed in L-hI93M mice at 20 weeks of age, we speculated that dopaminergic

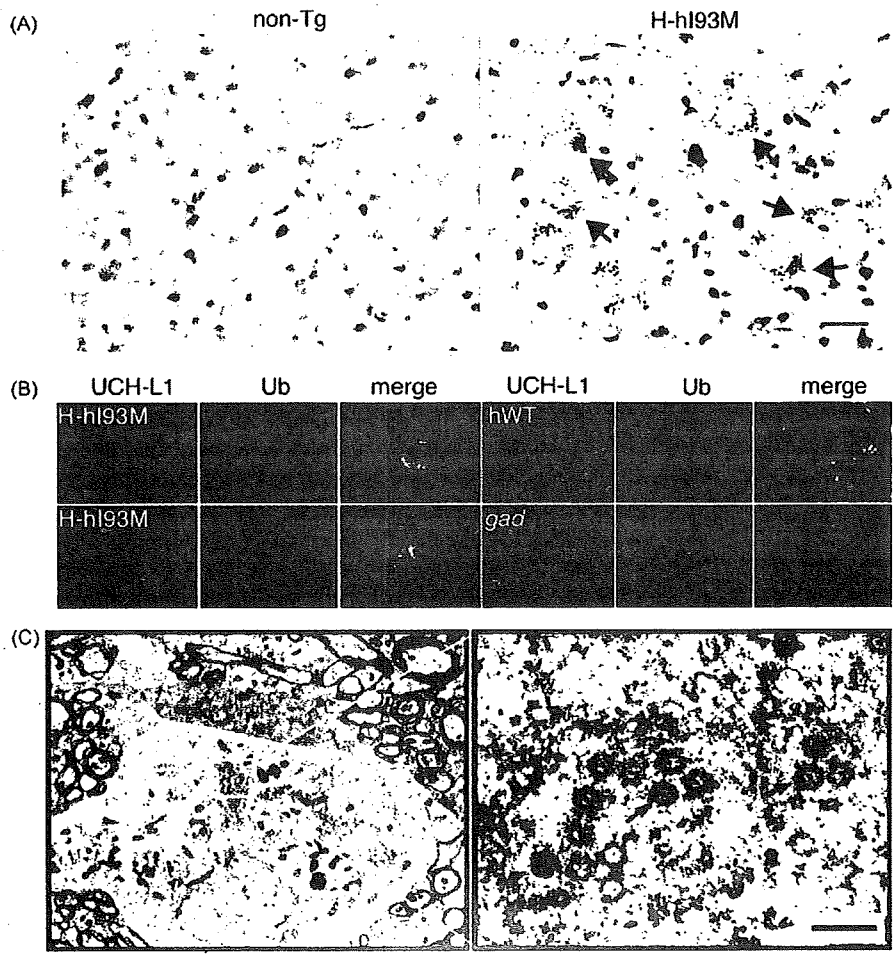

Fig. 4. Several neuropathological features reminiscent of PD are present in H-hI93M mice brains. (A) Silver staining of the substantia nigra at 12 weeks of age in non-Tg and H-hI93M mice. Note the presence of silver staining-positive argyrophilic grains in the cell bodies of some dopaminergic neurons in H-hI93M mice (arrows). This kind of abnormal structure was not seen in substantia nigra of non-Tg mice. Scale bar: 30 μm. (B) Confocal images of dopaminergic neurons from hWT, H-hI93M and *gad* mice. H-hI93M mice showed the formation of ubiquitin-positive cytoplasmic inclusions (red) co-localized with UCH-L1 staining (green) in the remaining nigral neurons at 20 weeks of age. Compared with the diffuse, reduced staining of ubiquitin in *gad* mice, nigral neurons from hWT mice also showed a diffuse pattern of staining but with fine small granular cytoplasmic staining (red) co-localized with UCH-L1 (green). (C) Electron micrographs of a nigral neuron from a 20-week-old H-hI93M mouse at the level of the cell body (left panel), and dense-core vesicles (red arrows) at higher magnification (right panel). Scale bar: 1 μm.

neurons of L-hI93M mice might be more susceptible to MPTP toxin compared to that of non-Tg mice or hWT mice. As expected, significantly fewer TH-positive neurons were observed in L-hI93M mice after MPTP treatment as compared with hWT or non-Tg control mice though hWT express higher *hUCHL1* compared to L-hI93M (Fig. 3C). The number of TH-positive neurons in MPTP-treated hWT mice was somewhat higher than that in non-Tg mice ($p < 0.001$). Taken together with the fact that expression of human UCH-L1 in L-hI93M is lower than that in hWT, these results suggest that the UCH-L1^{I93M} mutant, but not UCH-L1^{WT}, is specifically toxic to dopaminergic neurons.

3.3. Presence of neuropathology in dopaminergic neurons from H-hI93M mice

To evaluate the degenerative process of dopaminergic neurons, silver staining was used to indicate argyrophilic degenerating neurons (Lo Bianco et al., 2004). In non-Tg mice, no silver staining was observed, whereas scattered neurons containing grains that were silver staining positive were present in the substantia nigra of H-hI93M mice (Fig. 4A). The presence of intracellular inclusions called Lewy bodies and Lewy neurites are neuropathological characteristics of PD and are silver staining positive (Sandmann-Keil et al., 1999; Uchihara et al., 2005). It is also known that UCH-L1 and ubiquitin, as well as α-synuclein, are components of Lewy bodies (Lowe et al., 1990). Furthermore, UCH-L1 is tightly associated with mono-ubiquitin *in vivo* (Osaka et al., 2003). Thus, we expected that the silver staining-positive grains might have characteristic features of Lewy bodies. We therefore compared the immunohistochemical analysis of UCH-L1 and ubiquitin. Compared with reduced staining for ubiquitin in *gad* mice, strong and diffuse ubiquitin staining was observed in nigral neurons of hWT mice and non-Tg mice (data not shown), and this staining co-localized with UCH-L1, which is in agreement with our previous report (Osaka et al., 2003). In H-hI93M substantia nigra at 20 weeks of age, ubiquitin- and UCH-L1-positive cytoplasmic inclusions, a large aggregates with different morphology from small dots usually seen in hWT mice and non-Tg mice, were observed in a portion of the remaining nigral neurons (Fig. 4B). These inclusions were, however, α-synuclein or hematoxylin–eosin (HE) negative (data not shown). We could not observe UCH-L1- and ubiquitin-positive inclusions in L-hI93M mice (data not shown).

Another cellular characteristic of PD neuropathology is dense-core vesicles of about 80–200 nm in perikarya, which are frequently observed along with Lewy bodies in PD patients (Watanabe et al., 1977). We observed electron dense-core vesicles in the cytoplasm of ~30% of nigral neurons in H-hI93M mice using electron microscopy (Fig. 4C). In non-Tg mice, such vesicles with a similar shape were not detected in cell bodies but rather were seen in synaptic terminals. Taken together, our data indicate that degenerating dopaminergic neurons in the substantia nigra of H-hI93M mice are devoid of Lewy bodies but show some neuropathological features such as silver staining-positive argyrophilic grains, aggregates with UCH-L1 and ubiquitin, and dense-core vesicles in the perikarya.

3.4. Increased amount of SDS-insoluble but urea/SDS-soluble UCH-L1 in the midbrain of H-hI93M mice

UCH-L1^{I93M} has reduced α-helical content as compared with UCH-L1^{WT} (Nishikawa et al., 2003), and UCH-L1^{I93M} overexpression in COS7 cells results in more cells that contain cytoplasmic inclusions (Ardley et al., 2004). Thus, the presence of UCH-L1-positive inclusions in H-hI93M dopaminergic neurons led us to speculate whether UCH-L1^{I93M} would be less soluble than the wild-type protein *in vivo*. To biochemically characterize the changes in UCH-L1 deposited in the brains of H-hI93M mice, we sequentially extracted frozen midbrain tissues with 5% SDS (soluble fraction) and 8 M urea/5% SDS (insoluble fraction) and analyzed each fraction by immunoblotting with anti-UCH-L1. As expected, immunoblots of insoluble fractions showed a modest but statistically significant increase in UCH-L1 in the midbrains of H-hI93M mice as compared with those from a non-Tg mouse (Fig. 5A and B), indicating increased insolubility of UCH-L1^{I93M} *in vivo*, which might have resulted in dopaminergic neurotoxicity.

3.5. Decreased dopamine content in the striata of H-hI93M mice

Because the nigro-striatal pathway is severely affected in PD patients, and because our mice showed the degeneration of dopaminergic neurons in the substantia nigra, we evaluated the nerve terminals in the striatal pathway using

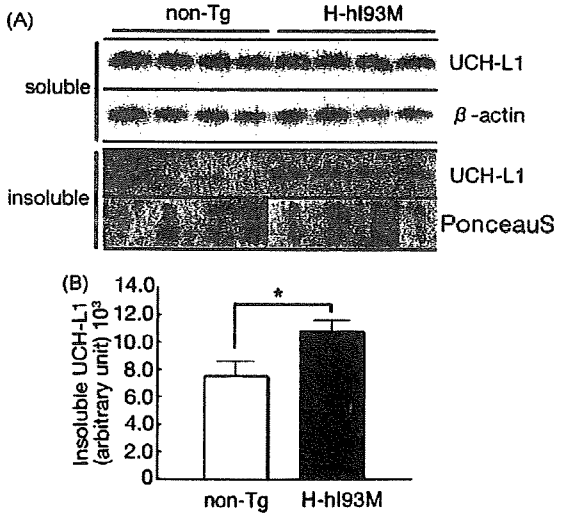

Fig. 5. Protein insolubility of UCH-L1 in H-hI93M Tg mice. (A) Immunoblotting analysis of UCH-L1 in soluble (5% SDS soluble) and insoluble (5% SDS insoluble and 8 M urea/5% SDS soluble) fractions from tissue containing the substantia nigra (11–13 weeks). Soluble fraction (5 μg for each) was probed with anti-UCH-L1 or anti-β-actin. Insoluble fraction (0.5 μg for each) was probed with anti-UCH-L1. One microgram of each insoluble fraction was applied to dot blotting and stained by Ponceau S to show that each fraction contained the same amount of total protein. A slight increase in the insolubility of UCH-L1 in the substantia nigra fraction from H-hI93M mice is seen as compared with that from non-Tg mice. (B) The experiment was done with H-hI93M mice and non-Tg littermates from five different litters, and the results of quantitative analyses in insoluble fraction is shown ($n = 5$ mice for each group).

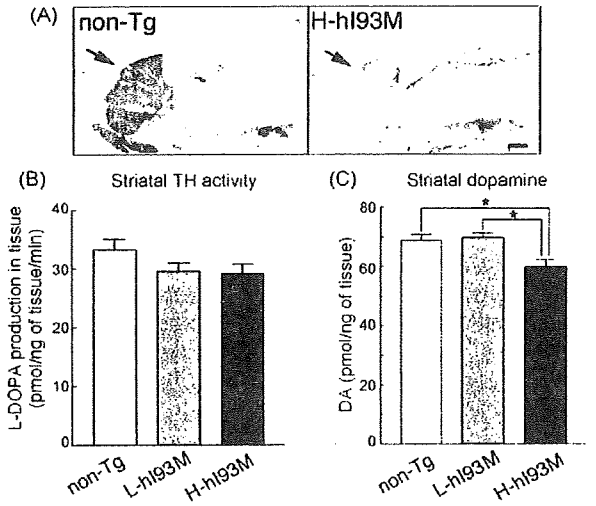

Fig. 6. H-hI93M mice show pathology in the striatum. Dopamine content and TH activity were lower in H-hI93M mice. (A) Sagittal sections from non-Tg and H-hI93M mice at 20 weeks of age were immunostained with the dopaminergic marker anti-TH. TH immunoreactivity is decreased in the nigro-striatal axons (arrows) of H-hI93M brains. Scale bar: 100 μm. (B) TH activity and (C) dopamine content were measured following extraction and homogenization of the mouse striatum of non-Tg, L-hI93M and H-hI93M mice at 20 weeks of age ($n = 4$; mean ± S.E). Significance was examined by a one-way ANOVA. $^{*}p < 0.05$.

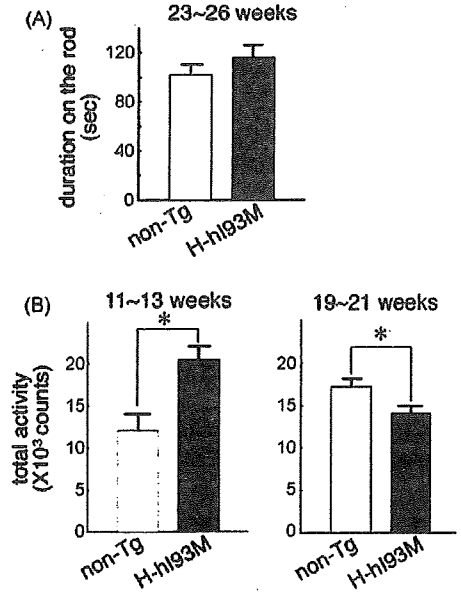

Fig. 7. H-hI93M transgenic mice show locomotor deficits. (A) Accelerated rota-rod analysis of H-hI93M and non-Tg mice ($n = 6$ for non-Tg and $n = 7$ for H-hI93M) at 23–26 weeks of age. Mice were placed on a rod, and their duration on the rod before falling off (mean value of three trials for each animal) was recorded. (B) Home cage monitor analysis of H-hI93M and non-Tg mice at 11–13 weeks of age (left; $n = 4$ for each line) and at 19–21 weeks of age (right; $n = 8$ for non-Tg and $n = 10$ for H-hI93M). Note the significant hypolocomotion of H-hI93M mice as compared with non-Tg mice at 19–21 weeks of age. Values are the mean ± S.E.M. Significance was examined using the unpaired Student's t-test. $^{*}p < 0.05$.

immunohistochemical and biochemical analyses. In agreement with the reduction of TH-positive dopaminergic neurons in the substantia nigra, nigro-striatal fibers in H-hI93M mice showed decreased immunoreactivity for TH as compared with that of non-Tg mice (Fig. 6A). TH activity, analyzed by determining L-DOPA production in the striatal tissues, also showed a tendency to decline in H-hI93M mice, although it was not significantly different (Fig. 6B). Loss of dopaminergic neurons in the substantia nigra and decreased TH activity in the striatum of H-hI93M mice prompted us to examine the concentration of striatal dopamine. Compared with non-Tg mice, H-hI93M mice showed a significant reduction of dopamine content in the striatum (Fig. 6C).

3.6. Decreased spontaneous, voluntary movements of H-hI93M mice

Given the prominent loss of dopaminergic neurons in the substantia nigra and the reduction in dopamine content in the striatum of H-hI93M mice, we next assessed the locomotor abilities of H-hI93M mice using a battery of well-established behavioral tests. Involuntary movement was analyzed by the rota-rod test (Goldberg et al., 2005) on 23–26-week-old mice. H-hI93M mice and non-Tg mice were similarly able to maintain their balance on the rotating rod during rod acceleration before falling off (Fig. 7A). We next analyzed spontaneous, voluntary movements with a locomotor activity test (Goldberg et al., 2005). Unexpectedly, 11–13-week-old H-hI93M mice showed significant hyperlocomotion during active periods (i.e., at night) as compared with non-Tg mice during home cage monitoring (Fig. 7B). However, 19–21-week-old H-hI93M mice showed a modest but significant reduction in locomotor activity during active periods as compared with non-Tg mice (Fig. 7B). These results indicate that, in addition to the neuropathological changes, H-hI93M mice exhibit mild behavioral deficits related to PD.

4. Discussion

In this study, we characterized transgenic mice expressing hUCH-L1^{I93M}, a mutation with presumptive association with familial PD, in the brain. Our previous attempt of making mouse UCH-L1^{WT} Tg mice under various higher expressing promoters, such as EF1α, resulted in an infertility of mice, thus it was impossible to maintain the lines. This failure resulted from the effect of overexpressing UCH-L1 in the testis/ovary leading to an increased apoptosis in these reproductive organs, although we did not find obvious morphological differences in the brain (Wang et al., 2006). Thus, we used *PDGF-B* promoter in this study to avoid massive expression of the transgene.

Two lines of hUCH-L1^{I93M} Tg mice and one line of hUCH-L1^{WT} Tg mice were viable and fertile without any predictable abnormalities. All of the three Tg lines expressed very limited levels of the human *UCHL1* gene with a maximum transcript ratio of about 1/100 as compared with the endogenous mouse *Uchl1*. However, immunohistological analysis indicated that higher level of hUCH-L1^{I93M} expression could be detected in the large number of neurons in the substantia nigra of

H-hI93M/gad mice at 2 weeks of age. In addition, there is a difference in the morphology of hUCH-L1^{I93M} expressing neurons, reminiscent of dying neurons, in the substantia nigra of H-hI93M/gad mice among 7 and 20 weeks of age. We also observed an eventual decline in the number of UCH-L1-positive neurons in H-hI93M/gad mice, as they age. Furthermore, the dopaminergic neurons in the substantia nigra of H-hI93M mice at 12 weeks of age showed silver staining-positive argylophilic grains, which represent neurons undergoing degeneration (Lo Bianco et al., 2004). Since we observed a loss of dopaminergic neurons in the substantia nigra and reduced dopamine content in the striatum of H-hI93M mice at 20 weeks of age, our results indicate the possibility that hUCH-L1^{I93M} expressing dopaminergic neurons degenerate with age.

In addition to cell loss, several neuropathological features were observed in the substantia nigra of H-hI93M mice. Dopaminergic neurons had (1) electron dense-core vesicles in the perikarya, and (2) cytoplasmic inclusions that were positive for both UCH-L1 and ubiquitin. Despite these features, we did not observe eosinophilic or α-synuclein-positive Lewy bodies at the substantia nigra in our morphological analyses. Thus, the mouse dopaminergic neurons expressing UCH-L1^{I93M} may die prior to the formation of Lewy bodies, or those mice might form these structures at stages beyond the period of our study.

The mechanisms responsible for dopaminergic cell loss in the substantia nigra of H-hI93M mice remain elusive. The I93M mutation in UCH-L1 reduces its hydrolase activity by about 50%, which has been suggested as a cause for the pathogenesis of PD (Nishikawa et al., 2003). However, we have not found clear evidence for nigro-striatal dopaminergic pathology in *gad* mice (data not shown). Since expression of UCH-L1 is not detected in gad mice, the reduction of hydrolase activity alone would not be the cause of PD. In light of our finding here that transgenic expression of UCH-L1^{I93M} results in dopaminergic pathology in mice, it would seem that this mutation elicits a gain of toxic function leading to the neuronal toxicity in the substantia nigra.

Our previous work using circular dichroism suggests that the I93M mutation reduces the α-helical content of UCH-L1 (Nishikawa et al., 2003). Recently, we had also showed, using small-angle neutron scattering, that wild-type or I93M mutant UCH-L1 exists as a dimmer in an aqueous solution. Moreover, their configuration differed; wild-type UCH-L1 has ellipsoidal shape where as I93M mutant has more globular shape (Naito et al., 2006). Cells expressing UCH-L1^{I93M} are more prone to form inclusions (Ardley et al., 2004). Proteomic analysis of autopsied brains from PD patients and AD patients shows that UCH-L1 is extensively modified by carbonyl formation, methionine oxidation and cysteine oxidation in the diseased brains (Choi et al., 2004). These modifications are shown to result from oxidative stress (Choi et al., 2004). We show here that I93M mutation in UCH-L1 increases its insolubility *in vivo*. From the very limited expression of human UCH-L1 I93M, it is possible to speculate that endogenous mouse UCH-L1 might become insoluble in the presence of I93M UCH-L1. In addition, L-hI93M neurons were more susceptible than hWT or non-Tg neurons to MPTP, an inhibitor of complex I. This observation suggests that UCH-L1^{I93M} easily gains toxicity under oxidative stress. The conformational change and/or the additional methionine oxidation in UCH-L1 caused by I93M mutation may cause increased insolubility and lead to the gain of a toxic function.

In addition, our behavioral analysis revealed that H-hI93M mice exhibit very slight defects in spontaneous, voluntary movement, as shown by their hyperlocomotion at 11–13 weeks of age and by their hypolocomotion at 19–21 weeks of age in the home cage monitor test. Patients with PD exhibit no clinical symptoms until 70–80% of dopaminergic neurons are lost (Dauer and Przedborski, 2003). Thus, the level of dopaminergic neuronal loss seen in H-hI93M mice might not be sufficient to produce severe clinical phenotypes. It is difficult to explain the hyperlocomotion detected at 11–13 weeks of age, by simple changes in the nigro-striatal pathway. Other brain areas might be related to the locomotor changes seen in H-hI93M mice. We will need further analysis to connect the dopaminergic cell loss and defects in spontaneous, voluntary movement in H-hI93M mice.

In attempts to replicate neuropathological aspects of PD, several of the familial PD genes have been altered in mice. Up to date, α-synuclein Tg mice with or without mutation (Fernagut and Chesselet, 2004), parkin knockout mice (Goldberg et al., 2003; Itier et al., 2003; Palacino et al., 2004; Perez and Palmiter, 2005; Von Coelln et al., 2004), and DJ-1 knockout mice (Chen et al., 2005; Goldberg et al., 2005; Kim et al., 2005) have been reported. Although these mice show some alterations in the function of dopaminergic neurons, none has dopaminergic neuron loss in the substantia nigra. Thus, we have developed the first mouse model with an alteration in a familial PD gene that leads to dopaminergic cell loss. Further analysis of these mice will help establish the role of UCH-L1 in PD, which may elucidate a common pathway for both familial and sporadic PD.

Acknowledgements

This work was supported by the Program for Promotion of Fundamental Studies in Health Sciences of the National Institute of Biomedical Innovation of Japan (KW); Grants-in-Aid for Scientific Research from the Ministry of Health, Labour and Welfare of Japan (KW); Grants-in-Aid for Scientific Research from the Ministry of Education, Culture, Sports, Science and Technology of Japan (KW); a grant from Japan Science and Technology Cooperation and a High Technology Research Center Grant (YM). We thank M. Shikama for the care and breeding of animals, H. Fujita for genotyping of animals, H. Kikuchi for technical assistance with tissue sections and N. Takagaki for the support in English. We also thank Dr. H. Hohjo for letting us use the home cage monitor.

References

Aoki, S., Su, Q., Li, H., Nishikawa, K., Ayukawa, K., Hara, Y., Namikawa, K., Kiryu-Seo, S., Kiyama, H., Wada, K., 2002. Identification of an axotomy-induced glycosylated protein, AIGP1, possibly involved in cell death triggered by endoplasmic reticulum-Golgi stress. J. Neurosci. 22, 10751–10760.

Ardley, H.C., Scott, G.B., Rose, S.A., Tan, N.G., Robinson, P.A., 2004. UCH-L1 aggresome formation in response to proteasome impairment indicates a role in inclusion formation in Parkinson's disease. J. Neurochem. 90, 379–391.

Bonifati, V., Rizzu, P., van Baren, M.J., Schaap, O., Breedveld, G.J., Krieger, E., Dekker, M.C., Squitieri, F., Ibanez, P., Joosse, M., van Dongen, J.W., Vanacore, N., van Swieten, J.C., Brice, A., Meco, G., van Duijn, C.M., Oostra, B.A., Heutink, P., 2003. Mutations in the DJ-1 gene associated with autosomal recessive early-onset parkinsonism. Science 299, 256–259.

Chartier-Harlin, M.C., Kachergus, J., Roumier, C., Mouroux, V., Douay, X., Lincoln, S., Levecque, C., Larvor, L., Andrieux, J., Hulihan, M., Waucquier, N., Defebvre, L., Amouyel, P., Farrer, M., Destee, A., 2004. Alpha-synuclein locus duplication as a cause of familial Parkinson's disease. Lancet 364, 1167–1169.

Chen, L., Cagniard, B., Mathews, T., Jones, S., Koh, H.C., Ding, Y., Carvey, P.M., Ling, Z., Kang, U.J., Zhuang, X., 2005. Age-dependent motor deficits and dopaminergic dysfunction in DJ-1 null mice. J. Biol. Chem. 280, 21418–21426.

Choi, J., Levey, A.I., Weintraub, S.T., Rees, H.D., Gearing, M., Chin, L.S., Li, L., 2004. Oxidative modifications and down-regulation of ubiquitin carboxyl-terminal hydrolase L1 associated with idiopathic Parkinson's and Alzheimer's diseases. J. Biol. Chem. 279, 13256–13264.

Dauer, W., Przedborski, S., 2003. Parkinson's disease: mechanisms and models. Neuron 39, 889–909.

Farrer, M., Kachergus, J., Forno, L., Lincoln, S., Wang, D.S., Hulihan, M., Maraganore, D., Gwinn-Hardy, K., Wszolek, Z., Dickson, D., Langston, J.W., 2004. Comparison of kindreds with parkinsonism and alpha-synuclein genomic multiplications. Ann. Neurol. 55, 174–179.

Fernagut, P.O., Chesselet, M.F., 2004. Alpha-synuclein and transgenic mouse models. Neurobiol. Dis. 17, 123–130.

Furuya, T., Hayakawa, H., Yamada, M., Yoshimi, K., Hisahara, S., Miura, M., Mizuno, Y., Mochizuki, H., 2004. Caspase-11 mediates inflammatory dopaminergic cell death in the 1-methyl-4-phenyl-1,2,3,6-tetrahydropyridine mouse model of Parkinson's disease. J. Neurosci. 24, 1865–1872.

Goldberg, M.S., Fleming, S.M., Palacino, J.J., Cepeda, C., Lam, H.A., Bhatnagar, A., Meloni, E.G., Wu, N., Ackerson, L.C., Klapstein, G.J., Gajendiran, M., Roth, B.L., Chesselet, M.F., Maidment, N.T., Levine, M.S., Shen, J., 2003. Parkin-deficient mice exhibit nigrostriatal deficits but not loss of dopaminergic neurons. J. Biol. Chem. 278, 43628–43635.

Goldberg, M.S., Pisani, A., Haburcak, M., Vortherms, T.A., Kitada, T., Costa, C., Tong, Y., Martella, G., Tscherter, A., Martins, A., Bernardi, G., Roth, B.L., Pothos, E.N., Calabresi, P., Shen, J., 2005. Nigrostriatal dopaminergic deficits and hypokinesia caused by inactivation of the familial Parkinsonism-linked gene DJ-1. Neuron 45, 489–496.

Hemelaar, J., Borodovsky, A., Kessler, B.M., Reverter, D., Cook, J., Kolli, N., Gan-Erdene, T., Wilkinson, K.D., Gill, G., Lima, C.D., Ploegh, H.L., Ovaa, H., 2004. Specific and covalent targeting of conjugating and deconjugating enzymes of ubiquitin-like proteins. Mol. Cell. Biol. 24, 84–95.

Hooper, D., Kawamura, M., Hoffman, B., Kopin, I.J., Hunyady, B., Mezey, E., Eisenhofer, G., 1997. Tyrosine hydroxylase assay for detection of low levels of enzyme activity in peripheral tissues. J. Chromatogr. B: Biomed. Sci. Appl. 694, 317–324.

Ibanez, P., Bonnet, A.M., Debarges, B., Lohmann, E., Tison, F., Pollak, P., Agid, Y., Durr, A., Brice, A., 2004. Causal relation between alpha-synuclein gene duplication and familial Parkinson's disease. Lancet 364, 1169–1171.

Itier, J.M., Ibanez, P., Mena, M.A., Abbas, N., Cohen-Salmon, C., Bohme, G.A., Laville, M., Pratt, J., Corti, O., Pradier, L., Ret, G., Joubert, C., Periquet, M., Araujo, F., Negroni, J., Casarejos, M.J., Canals, S., Solano, R., Serrano, A., Gallego, E., Sanchez, M., Denefle, P., Benavides, J., Tremp, G., Rooney, T.A., Brice, A., Garcia de Yebenes, J., 2003. Parkin gene inactivation alters behaviour and dopamine neurotransmission in the mouse. Hum. Mol. Genet. 12, 2277–2291.

Kahle, P.J., Neumann, M., Ozmen, L., Muller, V., Odoy, S., Okamoto, N., Jacobsen, H., Iwatsubo, T., Trojanowski, J.Q., Takahashi, H., Wakabayashi, K., Bogdanovic, N., Riederer, P., Kretzschmar, H.A., Haass, C., 2001. Selective insolubility of alpha-synuclein in human Lewy body diseases is recapitulated in a transgenic mouse model. Am. J. Pathol. 159, 2215–2225.

Kim, R.H., Smith, P.D., Aleyasin, H., Hayley, S., Mount, M.P., Pownall, S., Wakeham, A., You-Ten, A.J., Kalia, S.K., Horne, P., Westaway, D., Lozano, A.M., Anisman, H., Park, D.S., Mak, T.W., 2005. Hypersensitivity of DJ-1-deficient mice to 1-methyl-4-phenyl-1,2,3,6-tetrahydropyrindine (MPTP) and oxidative stress. Proc. Natl. Acad. Sci. U.S.A. 102, 5215–5220.

Kitada, T., Asakawa, S., Hattori, N., Matsumine, H., Yamamura, Y., Minoshima, S., Yokochi, M., Mizuno, Y., Shimizu, N., 1998. Mutations in the parkin gene cause autosomal recessive juvenile parkinsonism. Nature 392, 605–608.

Kruger, R., Kuhn, W., Muller, T., Woitalla, D., Graeber, M., Kosel, S., Przuntek, H., Epplen, J.T., Schols, L., Riess, O., 1998. Ala30Pro mutation in the gene encoding alpha-synuclein in Parkinson's disease. Nat. Genet. 18, 106–108.

Larsen, C.N., Krantz, B.A., Wilkinson, K.D., 1998. Substrate specificity of deubiquitinating enzymes: ubiquitin C-terminal hydrolases. Biochemistry 37, 3358–3368.

Leroy, E., Boyer, R., Auburger, G., Leube, B., Ulm, G., Mezey, E., Harta, G., Brownstein, M.J., Jonnalagada, S., Chernova, T., Dehejia, A., Lavedan, C., Gasser, T., Steinbach, P.J., Wilkinson, K.D., Polymeropoulos, M.H., 1998. The ubiquitin pathway in Parkinson's disease. Nature 395, 451–452.

Lincoln, S., Vaughan, J., Wood, N., Baker, M., Adamson, J., Gwinn-Hardy, K., Lynch, T., Hardy, J., Farrer, M., 1999. Low frequency of pathogenic mutations in the ubiquitin carboxy-terminal hydrolase gene in familial Parkinson's disease. Neuroreport 10, 427–429.

Liu, Y., Fallon, L., Lashuel, H.A., Liu, Z., Lansbury Jr., P.T., 2002. The UCH-L1 gene encodes two opposing enzymatic activities that affect alpha-synuclein degradation and Parkinson's disease susceptibility. Cell 111, 209–218.

Lo Bianco, C., Schneider, B.L., Bauer, M., Sajadi, A., Brice, A., Iwatsubo, T., Aebischer, P., 2004. Lentiviral vector delivery of parkin prevents dopaminergic degeneration in an alpha-synuclein rat model of Parkinson's disease. Proc. Natl. Acad. Sci. U.S.A. 101, 17510–17515.

Lowe, J., McDermott, H., Landon, M., Mayer, R.J., Wilkinson, K.D., 1990. Ubiquitin carboxyl-terminal hydrolase (PGP 9.5) is selectively present in ubiquitinated inclusion bodies characteristic of human neurodegenerative diseases. J. Pathol. 161, 153–160.

Maraganore, D.M., Farrer, M.J., Hardy, J.A., Lincoln, S.J., McDonnell, S.K., Rocca, W.A., 1999. Case-control study of the ubiquitin carboxy-terminal hydrolase L1 gene in Parkinson's disease. Neurology 53, 1858–1860.

Mochizuki, H., Hayakawa, H., Migita, M., Shibata, M., Tanaka, R., Suzuki, A., Shimo-Nakanishi, Y., Urabe, T., Yamada, M., Tamayose, K., Shimada, T., Miura, M., Mizuno, Y., 2001. An AAV-derived Apaf-1 dominant negative inhibitor prevents MPTP toxicity as antiapoptotic gene therapy for Parkinson's disease. Proc. Natl. Acad. Sci. U.S.A. 98, 10918–10923.

Naito, S., Mochizuki, H., Yasuda, T., Mizuno, Y., Furusaka, M., Ikeda, S., Adachi, T., Shimizu, H.M., Suzuki, J., Fujiwara, S., Okada, T., Nishikawa, K., Aoki, S., Wada, K., 2006. Characterization of multimetric variants of ubiquitin carboxyl-terminal hydrolase L1 in water by small-angle neutron scattering. Biochem. Biophys. Res. Commun. 339, 717–725.

Naoi, M., Takahashi, T., Nagatsu, T., 1988. Simple assay procedure for tyrosine hydroxylase activity by high-performance liquid chromatography employing coulometric detection with minimal sample preparation. J. Chromatogr. 427, 229–238.

Nishikawa, K., Li, H., Kawamura, R., Osaka, H., Wang, Y.L., Hara, Y., Hirokawa, T., Manago, Y., Amano, T., Noda, M., Aoki, S., Wada, K., 2003. Alterations of structure and hydrolase activity of parkinsonism-associated human ubiquitin carboxyl-terminal hydrolase L1 variants. Biochem. Biophys. Res. Commun. 304, 176–183.

Osaka, H., Wang, Y.L., Takada, K., Takizawa, S., Setsuie, R., Li, H., Sato, Y., Nishikawa, K., Sun, Y.J., Sakurai, M., Harada, T., Hara, Y., Kimura, I., Chiba, S., Namikawa, K., Kiyama, H., Noda, M., Aoki, S., Wada, K., 2003. Ubiquitin carboxy-terminal hydrolase L1 binds to and stabilizes monoubiquitin in neuron. Hum. Mol. Genet. 12, 1945–1958.

Paisan-Ruiz, C., Jain, S., Evans, E.W., Gilks, W.P., Simon, J., van der Brug, M., Lopez de Munain, A., Aparicio, S., Gil, A.M., Khan, N., Johnson, J., Martinez, J.R., Nicholl, D., Carrera, I.M., Pena, A.S., de Silva, R., Lees, A., Marti-Masso, J.F., Perez-Tur, J., Wood, N.W., Singleton, A.B., 2004. Cloning of the gene containing mutations that cause PARK8-linked Parkinson's disease. Neuron 44, 595–600.

Palacino, J.J., Sagi, D., Goldberg, M.S., Krauss, S., Motz, C., Wacker, M., Klose, J., Shen, J., 2004. Mitochondrial dysfunction and oxidative damage in parkin-deficient mice. J. Biol. Chem. 279, 18614–18622.

Perez, F.A., Palmiter, R.D., 2005. Parkin-deficient mice are not a robust model of parkinsonism. Proc. Natl. Acad. Sci. U.S.A. 102, 2174–2179.

Polymeropoulos, M.H., Lavedan, C., Leroy, E., Ide, S.E., Dehejia, A., Dutra, A., Pike, B., Root, H., Rubenstein, J., Boyer, R., Stenroos, E.S., Chandrasekharappa, S., Athanassiadou, A., Papapetropoulos, T., Johnson, W.G., Lazzarini, A.M., Duvoisin, R.C., Di Iorio, G., Golbe, L.I., Nussbaum, R.L., 1997. Mutation in the alpha-synuclein gene identified in families with Parkinson's disease. Science 276, 2045–2047.

Rane, N.S., Yonkovich, J.L., Hegde, R.S., 2004. Protection from cytosolic prion protein toxicity by modulation of protein translocation. EMBO J. 23, 4550–4559.

Saigoh, K., Wang, Y.L., Suh, J.G., Yamanishi, T., Sakai, Y., Kiyosawa, H., Harada, T., Ichihara, N., Wakana, S., Kikuchi, T., Wada, K., 1999. Intragenic deletion in the gene encoding ubiquitin carboxy-terminal hydrolase in gad mice. Nat. Genet. 23, 47–51.

Sandmann-Keil, D., Braak, H., Okochi, M., Haass, C., Braak, E., 1999. Alpha-synuclein immunoreactive Lewy bodies and Lewy neurites in Parkinson's disease are detectable by an advanced silver-staining technique. Acta Neuropathol. (Berl.) 98, 461–464.

Sasahara, M., Fries, J.W., Raines, E.W., Gown, A.M., Westrum, L.E., Frosch, M.P., Bonthron, D.T., Ross, R., Collins, T., 1991. PDGF B-chain in neurons of the central nervous system, posterior pituitary, and in a transgenic model. Cell 64, 217–227.

Singleton, A.B., Farrer, M., Johnson, J., Singleton, A., Hague, S., Kachergus, J., Hulihan, M., Peuralinna, T., Dutra, A., Nussbaum, R., Lincoln, S., Crawley, A., Hanson, M., Maraganore, D., Adler, C., Cookson, M.R., Muenter, M., Baptista, M., Miller, D., Blancato, J., Hardy, J., Gwinn-Hardy, K., 2003. Alpha-synuclein locus triplication causes Parkinson's disease. Science 302, 841.

Uchihara, T., Nakamura, A., Mochizuki, Y., Hayashi, M., Orimo, S., Isozaki, E., Mizutani, T., 2005. Silver stainings distinguish Lewy bodies and glial cytoplasmic inclusions: comparison between Gallyas-Braak and Campbell-Switzer methods. Acta Neuropathol. (Berl.) 110, 255–260.

Valente, E.M., Abou-Sleiman, P.M., Caputo, V., Muqit, M.M., Harvey, K., Gispert, S., Ali, Z., Del Turco, D., Bentivoglio, A.R., Healy, D.G., Albanese, A., Nussbaum, R., Gonzalez-Maldonado, R., Deller, T., Salvi, S., Cortelli, P., Gilks, W.P., Latchman, D.S., Harvey, R.J., Dallapiccola, B., Auburger, G., Wood, N.W., 2004. Hereditary early-onset Parkinson's disease caused by mutations in PINK1. Science 304, 1158–1160.

Vila, M., Przedborski, S., 2004. Genetic clues to the pathogenesis of Parkinson's disease. Nat. Med. 10 (Suppl.), S58–S62.

Von Coelln, R., Thomas, B., Savitt, J.M., Lim, K.L., Sasaki, M., Hess, E.J., Dawson, V.L., Dawson, T.M., 2004. Loss of locus coeruleus neurons and reduced startle in parkin null mice. Proc. Natl. Acad. Sci. U.S.A. 101, 10744–10749.

Wang, Y.L., Liu, W., Sun, Y.J., Kwon, J., Setsuie, R., Osaka, H., Noda, M., Aoki, S., Yoshikawa, Y., Wada, K., 2006. Overexpression of ubiquitin carboxyl-terminal hydrolase L1 arrests spermatogenesis in transgenic mice. Mol. Reprod. Develop. 73, 40–49.

Wang, Y.L., Takeda, A., Osaka, H., Hara, Y., Furuta, A., Setsuie, R., Sun, Y.J., Kwon, J., Sato, Y., Sakurai, M., Noda, M., Yoshikawa, Y., Wada, K., 2004. Accumulation of beta- and gamma-synucleins in the ubiquitin carboxyl-terminal hydrolase L1-deficient gad mouse. Brain Res. 1019, 1–9.

Watanabe, I., Vachal, E., Tomita, T., 1977. Dense core vesicles around the Lewy body in incidental Parkinson's disease: an electron microscopic study. Acta Neuropathol. (Berl.) 39, 173–175.

Wilkinson, K.D., Lee, K.M., Deshpande, S., Duerksen-Hughes, P., Boss, J.M., Pohl, J., 1989. The neuron-specific protein PGP 9.5 is a ubiquitin carboxyl-terminal hydrolase. Science 246, 670–673.

Zimprich, A., Biskup, S., Leitner, P., Lichtner, P., Farrer, M., Lincoln, S., Kachergus, J., Hulihan, M., Uitti, R.J., Calne, D.B., Stoessl, A.J., Pfeiffer, R.F., Patenge, N., Carbajal, I.C., Vieregge, P., Asmus, F., Muller-Minsk, B., Dickson, D.W., Meeting, T., Strom, T.M., Wszolek, Z.K., Gasser, T., 2004. Mutations in LRRK2 cause autosomal-dominant parkinsonism with allomorphic pathology. Neurone 44, 601–607.

GLIA 55:317–327 (2007)

PACAP/PAC1 Autocrine System Promotes Proliferation and Astrogenesis in Neural Progenitor Cells

MIKA NISHIMOTO,[1,2] AKIKO FURUTA,[1] SHUNSUKE AOKI,[1,3,4] YOSHIHISA KUDO,[2] HIROYOSHI MIYAKAWA,[2] AND KEIJI WADA[1,4*]

[1]*Department of Degenerative Neurological Diseases, National Institute of Neuroscience, National Center of Neurology and Psychiatry, Kodaira, Tokyo, Japan*

[2]*Laboratory of Cellular Neurobiology, Tokyo University of Pharmacology and Life science, Hachioji, Tokyo, Japan*

[3]*NEDO (New Energy and Industrial Technology Development Organization), Kawasaki, Kanagawa, Japan*

[4]*Core Research for Evolutional Science and Technology (CREST), Japan Science and Technology Agency (JST), Kawaguchi, Saitama, Japan*

KEY WORDS

pituitary adenylate cyclase-activating polypeptide (PACAP); PAC1; neural progenitor cell; autocrine proliferation factor

ABSTRACT

The Pituitary adenylate cyclase-activating peptide (PACAP) ligand/type 1 receptor (PAC1) system regulates neurogenesis and gliogenesis. It has been well established that the PACAP/PAC1 system induces differentiation of neural progenitor cells (NPCs) through the Gs-mediated cAMP-dependent signaling pathway. However, it is unknown whether this ligand/receptor system has a function in proliferation of NPCs. In this study, we identified that PACAP and PAC1 were highly expressed and co-localized in NPCs of mouse cortex at embryonic day 14.5 (E14.5) and found that the PACAP/PAC1 system potentiated growth factor-induced proliferation of mouse cortical NPCs at E14.5 via Gq-, but not Gs-, mediated PLC/IP_3-dependent signaling pathway in an autocrine manner. Moreover, PAC1 activation induced elongation of cellular processes and a stellate morphology in astrocytes that had the bromodeoxyuridine (BrdU)-incorporating ability of NPCs. Consistent with this notion, we determined that the most BrdU positive NPCs differentiated to astrocytes through PAC1 signaling. These results suggest that the PACAP/PAC1 system may play a dual role in neural/glial progenitor cells not only differentiation but also proliferation in the cortical astrocyte lineage via Ca^{2+}-dependent signaling pathways through PAC1.

INTRODUCTION

Multipotent and proliferative neural progenitor cells (NPCs) represent the epigenetic and intrinsic origin of neurons, astrocytes, and oligodendrocytes in the central nervous system (CNS) (Altman and Bayer, 1990a,b; Reynolds et al., 1992; Reynolds and Weiss, 1996). During brain development, neurogenesis and gliogenesis occur as distinct temporal events with only some overlap. In the mouse embryonic cortex, neurogenesis takes place between embryonic days (E) 12 and 17 to generate neurons from neuronal progenitors. In contrast, astrocytic differentiation begins mainly at E16 and continues in the postnatal days. In each embryonic stage, NPC proliferation or differentiation is mostly regulated by locally produced or peripherally circulating soluble paracrine factors such as growth factors (e.g. basic fibroblast growth factor (b-FGF) and epidermal growth factor (EGF)) and cytokines as well as several autocrine factors such as bone morphogenic protein-4 (BMP4), interleukin 6, glycosylated cystatin C, and insulin-like growth factors (Eccleston et al., 1991; Liu et al., 2004; Wislet-Gendebien et al., 2004). Although glial progenitors are known to arise from NPCs predominantly at a delay on neurogenesis, the underlying spatiotemporal regulatory mechanisms of proliferation and differentiation of glial progenitors are not yet defined.

The effects of pituitary adenylate cyclase-activating peptide (PACAP) and vasoactive intestinal peptide (VIP), which are members of the VIP/secretin/glucagon peptide family have been well characterized in the CNS. For example, these factors affect neurotransmitter release and survival of hippocampal neurons as well as controlling cerebellar maturation (Arimura, 1998; Basille et al., 1993; Bluet-Pajot et al., 1998; Otto et al., 2001; Rayan et al., 1991; Vaudry et al., 2002; Zhou et al., 2002). These PACAP and VIP functions are mediated by three PACAP receptors, PAC1, VPAC1, and VPAC2 (Christophe, 1993; Muller et al., 1995; Tatsuno et al., 1994; Zhou et al., 2002). In particular, PACAP and PAC1 are highly expressed and distributed ubiquitously in the embryonic CNS and peripheral nervous system (Tatsuno et al., 1994; Zhou et al., 2002). Accordingly, PACAP is considered to influence the regulation of NPC proliferation and/or differentiation during embryonic development (Dicicco-Bloom et al., 1998). The PAC1 gene encodes a

Grant sponsors: Grants-in Aid for Scientific Research, Japanese Society for Promotion of Science; Research Grant in Priority Area Research, Ministry of Education, Culture, Sports, Science and Technology, Japan; Grants-in-Aid for Scientific Research, Ministry of Health, Labour and Welfare, Japan; CREST, Japanese Science and Technology Agency; Program for Promotion of Fundamental Studies, National Institute of Biomedical Innovation (NIBIO).

*Correspondence to: Keiji Wada, Department of Degenerative Neurological Diseases, National Institute of Neuroscience, National Center of Neurology and Psychiatry (NCNP), Kodaira 4-1-1, Tokyo 187-8502, Japan. E-mail: wada@ncnp.go.jp

Received 22 June 2006; Revised 18 October 2006; Accepted 20 October 2006

DOI 10.1002/glia.20461

Published online 17 November 2006 in Wiley InterScience (www.interscience.wiley.com).

G-protein-coupled receptor that has four splice variants, depending on the presence or absence of either one or two of the cassettes, "hip" and "hop," in the third intercellular loop (Bresson-Bepoldin et al., 1998; Jaworski and Proctor, 2000; Zhou et al., 2000a,b). These splice variants are involved in multiple and response-specific second messenger cascades (Pisegna et al., 1996). Evidence from studies with transfected cells indicates that each splice variant activates different cell signaling pathways involving adenylate cyclase (AC) and/or phospholipase C (PLC) and activation of these two pathways has opposite effects on the proliferation of cerebral cortical precursor cells (Basille et al., 1995; Cazillis et al., 2004; Lu et al., 1998; Mercer et al., 2004; Suh et al., 2001; Waschek et al., 2000). Recently it was shown that the PACAP/PAC1 system inhibits NPC proliferation and promotes neurogenesis and gliogenesis by activation of the Gs-mediated cAMP-dependent signal transduction pathway in the embryonic brain (Lelievre et al., 2002; Suh et al., 2001; Waschek et al., 1998). In contrast, PACAP was reported to promote adult NPC proliferation via PAC1 both in vivo and in vitro. Thus the precise effect of direct activation of PAC1 signaling on embryonic NPCs, and the mechanism thereof, remains unknown.

To elucidate the function of PACAP in embryonic cortical NPCs, we investigated regulatory mechanisms of PAC1 signaling for cell proliferation and differentiation using NPCs of mouse cortex at E14.5 when cortical NPCs in the ventricular zone (VZ)/subventricular zone (SVZ) contain not only neuronal progenitors but also glial progenitors. In this study, we identified that PACAP and PAC1 were highly expressed and co-localized in NPCs. Surprisingly, we found that the PACAP/PAC1 system potentiated growth factor-induced proliferation in mouse cortical NPCs at E14.5 via Gq-mediated—but not Gs-mediated—PLC/IP_3-dependent signaling pathways in an autocrine manner. Moreover, we showed that direct activation of PAC1 induced astrocyte-like morphological changes in embryonic cortical NPCs. Together with our present results and the previously identified role of PACAP, we suggest a dual role of the PACAP/PAC1 system for NPC proliferation during cortical astrogenesis by different signaling pathways of PAC1 variants at E14.5.

MATERIALS AND METHODS

Antibodies and Reagents

Monoclonal and polyclonal antibodies used in this study were as follows: mouse monoclonal anti-nestin (Becton Dickinson, Lexington, KY, and RaZ 401; Developmental Studies Hybridema Bank, Iowa City, IA), mouse monoclonal anti-neuronal class III β-tubulin (anti-β III tubulin (Tuj1); COVANCE, Berkeley, CA), mouse monoclonal anti-galactocerebroside (anti-Gal C; Chemicon International, Temecula, CA), rabbit polyclonal anti-glial fibrillary acidic protein (anti-GFAP: DAKO, Carpinteria, CA), goat polyclonal anti-PAC1 (gift from A. Arimura, Tulane University, New Orleans), rabbit polyclonal anti-PACAP38 (Calbiochem, San Diego, CA), rat monoclonal anti-bromodeoxyuridine (BrdU; Becton Dickinson, Lexington, KY). The secondary antibodies conjugated to Alexa Fluor fluorescein (goat anti-mouse Alexa Fluor 488, 568, or 633, goat anti-rabbit Alexa Fluor 488 or 568, rabbit anti-goat Alexa Fluor 594, and goat anti-mouse Alexa Fluor 488 or 568) were purchased from Molecular Probes (Eugene, OR). PACAP38, PACAP(6–38) (Peptide Institute, Osaka, Japan), VIP (Sigma, St. Louis, MO), maxadilan and M65 (gifts from Dr. Richard G. Titus, Colorado State University) were dissolved in distilled water. H89, 2-aminoethoxydiphenyl borate (2-APB; Calbiochem, San Diego, CA), chelerythrine (Sigma) and *O,O′*-bis(2-aminophenyl)ethyleneglycol-*N,N,N′,N′*-tetraacetic acid (BAPTA-AM; Sigma) were dissolved in DMSO. Each solution was added to the medium, and the final concentration of organic solvent (DMSO) in the medium was adjusted to no more than 0.1% (v/v). Each control medium contained the same amount of each organic solvent.

Animals

Pregnant C57BL/6J mice were purchased from CLEA Japan. All experiments were performed in the laboratory for animal experiments according to NIH Standards for Treatment of Laboratory Animals.

Culture of Mouse Embryonic Cortical NPCs

Cortical NPCs were cultured as previously described (Li et al., 2001; Nakashima et al., 1999). Briefly, embryos were removed from pregnant C57BL/6J mice (CLEA Japan, Tokyo, Japan) and staged according to morphological criteria to confirm gestational day (Kaufman, 1998). Developing mouse cerebral cortices were dissected at embryonic day 14.5 (E14.5). Cells were mechanically dissociated by trituration and plated at a density of 3.0×10^6 cells in 10-cm dishes (BD) that were precoated with 15 μg/mL poly-×L-ornithine (Sigma) and 1 μg/mL fibronectin (Nitta Gelatin, Osaka, Japan). Cells were expanded for 4 days in serum-free Neurobasal (NB) medium (Invitrogen, Carlsbad, CA) supplemented with B27 (Invitrogen), 0.5 mM L-glutamine (Invitrogen), 100 μg/mL penicillin and 100 μg/mL streptomycin (Invitrogen). This medium was supplemented with 10 ng/mL b-FGF (PeproTech, Rocky Hill, NJ), except where indicated otherwise. Cultures were maintained at 37°C in an atmosphere of 95% air and 5% CO_2. For secondary culture, b-FGF-expanded cortical NPCs were washed in warm Hanks' balanced salt solution, detached via mechanically pipetting, and resuspended in NB medium. Cells were then reseeded in 24-well plates (Nunc; 1×10^5 cells per well), 48-well plates (Nunc; 4.5×10^4 cells/well) or 96-well plates (Nunc; 1×10^4 cells/well) precoated with poly-L-ornithine and fibronectin.

Conditioned Medium Preparation

Subconfluent embryonic cortical NPCs in secondary cultures and control cultures maintained without

NvvPCs were incubated in serum-free NB/B27 medium for 48 h with b-FGF (5 ng/mL). After this period, conditioned medium derived from either NPCs or control cultures was collected and centrifuged at 1,000*g* for 5 min at 4°C to remove nonadherent cells.

Real-Time RT-PCR

Total RNA was isolated from cultured embryonic cortical NPCs and E14 mouse cerebral cortex. These RNAs (1 μg) were treated with DNase I and converted to cDNA using Superscript reverse transcriptase (Invitrogen) and random hexamer primers, according to the manufacturer's instructions. Real-time quantitative RT-PCR was performed with the SYBR Green-based method (ABI PRISM 7700 Sequence Detection System, Perkin-Elmer). The quantitative RT-PCR method (User Bulletin no. 2, Applied Biosystems, Foster City, CA) was modified to establish an expression level index for mRNA, and the SYBR green signal for the hypoxanthine-guanine phosphoribosyl transferase (hprt) gene amplicon was used as a reference. Amplification efficiency was determined and confirmed in a control PCR experiment using serially diluted cDNAs as templates. Real-time RT-PCR reactions were run on an ABI PRISM 7700 Sequence Detection System device using the following program: 2 min at 50°C, 10 min at 95°C and 40 cycles of 15 s at 95°C and 1 min at 60°C. The real-time RT-PCR products were analyzed using the sequence detection system software 1.7 (Applied Biosystems). The analysis and calculations were performed as described above. The efficiency of reverse transcription and the quality of cDNA was assessed by the efficiency of amplification of the hprt gene (upper primer, 5′-TCTTTGCTGACCTGCTGGATT-3′, corresponding to bases 222–241; lower, 5′-TATGTCCCC-CGTTGACTGATC-3′, corresponding to bases 322–342, GenBank accession no. NM-013556). PCR amplification was then performed with specific primers for PAC1, VPAC1, VPAC2, PACAP, and VIP, for which primers were designed using Primer Express software (Perkin-Elmer, Torrance, CA), as follows. PAC1: upper, 5′-CTT-CGATGCTTGTGGGTTTGA-3′, corresponding to bases 543–563 and lower, 5′-AAGCGGCACAAGATGACCAT-3′, bases 667–686, GenBank accession no. D82935; VPAC1: upper, 5′-TCCCCCATTCACGGCTATAA-3′, bases 413–423, and lower, 5′-CAGTCTGTTGCTGCTCATCCAT-3′, bases 525–540, GenBank accession no. NM011703; VPAC2: upper, 5′-CTTCTCCAGATGTTGGTGGCA-3′, bases 981–1,001, and lower, 5′-CCAATAGGGAAGGCAGCAAAC-3′, bases 1,078–1,098, GenBank accession no. D28132; PACAP: upper, 5′-GGCATGTGGGACAATATCACAT-3′, bases 319–340, and lower, 5′-ACTTGGTCCGGGTTGA-AGATC-3′, bases 399–419, GenBank accession no. NM009625; VIP: upper, 5′-GGAACAGACTGGTGGAGC-CTT-3′, bases 55–75, and lower, 5′-TTCCATCTCGGTG-CCTCCT-3′, bases 152–170, GenBank accession no. NM011702. To determine the expression of PAC1 splice variants, we used primer pairs and the condition of PCR amplification described previously (Jamen et al., 2002). A scheme for the design of primers for PAC1 splice variants is shown in Fig. 5A. For short or hip-hop variants: upper, 5′-CATCCTTGTGCAGAAGCTGC-3′, corresponding to bases 1,456–1,475, and lower, 5′-GGTGCTTGA-AGTCCATAGTG-3′, bases 1,825–1,844; hip variants: upper, 5′-ACAAATTTAAGACTGAGAGT-3′, bases 1,456–1,475, and lower, 5′-GGTGCTTGAAGTCCATAGTG-3′, bases 1,825–1,844. PCR was performed with an initial step at 94°C for 5 min followed by 35 cycles of 94°C for 30 s, 55°C for 30 s, 72°C for 1 min, and then a final cycle of 72°C for 10 min. Amplification products were stored at 4°C and then electrophoresed on a 2% agarose gel; the bands were visualized by ethidium bromide staining.

Immunohistochemistry and Immunocytochemistry

On embryonic day 14.5, C57BL/6J mouse brains were removed and fixed with 4% paraformaldehyde (PFA) for 8 h, cryoprotected in 20% sucrose in PBS, and frozen. Twenty-micrometer-thick coronal sections were cut with a cryostat, placed on APS-coated glass slides and then fixed with 4% PFA, washed three times with PBS, permeabilized with 0.1% (w/v) Triton X-100/PBS for 5 min and finally washed three times with PBS. Fixed sections were incubated for 30 min with 3% bovine serum albumin (Sigma). Sections were incubated overnight at 4°C with diluted primary polyclonal anti-PAC1 (1:1,000), see earlier for manufacturer's details, anti-PACAP38 (1:1,000) and anti-nestin (1:500) for triple staining. These sections were incubated for 1 h with diluted secondary antibodies (goat anti-mouse Alexa Fluor 633, goat anti-rabbit Alexa Fluor 488, and rabbit anti-goat Alexa Fluor 594) and washed with PBS. Confocal microscopy was performed using the Leica TCS SP2 spectral confocal scanning system (Leica Microsystems). For immunofluorescence measurements, cultured mouse embryonic NPCs were grown on poly-L-ornithine- and fibronectin-coated dishes. All incubations and washes were performed at room temperature. Cells were fixed with 4% PFA, washed three times with PBS, permeabilized with 0.1% Triton X-100/PBS for 5 min and then washed three times with PBS. Fixed cells were incubated for 30 min with 3.3% goat or rabbit serum (Nichirei, Tokyo, Japan). Cells were incubated for 0.5–1 h with diluted primary polyclonal or monoclonal antibody (both were used for double-staining). Next, these cells were incubated for 0.5–1 h with diluted secondary antibodies conjugated to fluorescein and washed with PBS. For BrdU labeling, cells were incubated with 2 M HCl at 37°C for 30 min, rinsed in 0.1 M sodium borate buffer and processed for immunocytochemistry. As a negative control in immunohistochemistry and immunocytochemistry, we performed the omission of either primary or secondary antibodies. Confocal microscopy was performed using the FLUOVIEW confocal microscope system (Olympus, Tokyo, Japan).